EFFECT OF CD320 KO ON CELL PROLIFERATION OF LUNG CANCER CELLS

by

Agiman Khalimov

A Thesis Submitted to the School of Medicine of Nazarbayev University in Partial Fulfillment of the Requirements for the Degree of

Master of Science in Molecular Medicine

at

NAZARBAYEV UNIVERSITY

SCHOOL OF MEDICINE

ASTANA, KAZAKHSTAN

2025

EFFECT OF CD320 KO ON CELL PROLIFERATION OF LUNG CANCER CELLS

by

Agiman Khalimov

Principal Investigator: Larisa Lezina

Electronic Version Approved:

Prof. Nikolai Barlev,

Director of the Master's in Molecular Medicine program

in School of Medicine

Nazarbayev University

April 2025

DECLARATION

I hereby declare that the thesis is my original work, and it has been written by me in its entirety. I have duly acknowledged all the sources of information that have been used in the thesis. This thesis has also not been submitted for any degree at any university previously.

Student name: Agiman Khalimov

Date: 02.05.25

Signature: 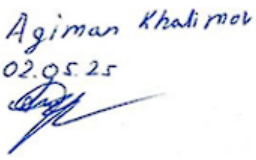

THESIS APPROVAL FORM

NAZARBAYEV UNIVERSITY

SCHOOL OF MEDICINE

EFFECT OF CD320 KO ON CELL PROLIFERATION OF LUNG CANCER CELLS

by

AGIMAN KHALIMOV

NU student number: 202325517

ORCID number: 0009-0002-6971-9788

APPROVED

BY

PROFESSOR NIKOLAI BARLEV, DIRECTOR OF THE

MASTER IN MOLECULAR MEDICINE PROGRAM

ON

The 3rd day of May, 2025.

_____

Signature of Principal Thesis Adviser

Master Thesis

Title: Effect of CD320 KO on cell proliferation of lung cancer cells

Abstract

Mutations in the TP53 tumor suppressor gene are the most common genetic alteration found in human cancers, identified in almost half of human malignancies. Other tumor suppressors (e.g., RB, APC, and BRCA1) are usually inactivated through frameshift or nonsense mutations; however, the majority of TP53 mutations (approximately 80%) are missense mutations resulting in a p53 protein that can exhibit altered and potentially deleterious functions. Some reports have described mutant p53 variants that can act in concert with cancer progression. These gain-of-function mutants, like R273H and M246I, turn p53 from "a brake to an accelerator" – no longer stopping tumors, but stepping on the gas, especially in non-small cell lung cancer (NSCLC), where they are associated with aggressive phenotypes and resistance to therapy.

CD320, a receptor for the uptake of cobalamin (vitamin B12) by binding transcobalamin, is upregulated in rapidly proliferating cells, including various cancers. Its role in cancer proliferation makes it a promising target for therapeutic intervention.

Recent unpublished work from Dr. Larisa Lezina's lab has shown that TP53 GOF mutations lead to CD320 upregulation in non-small cell lung cancer (NSCLC) cells. However, this raises the critical questions: how does mutant p53 regulate CD320 transcription or translation?

To investigate this, the study will generate CRISPR/Cas9-based CD320 knockout NSCLC cell lines to analyze the transcriptional and translational consequences of p53 GOF mutations on CD320 expression. From this work, we hope to clarify the oncogenic relationship between mutant p53 and CD320, and provide molecular bases that may lead to new, specific targeting therapies in cancers with such activating mutations.

List of keywords: p53, CD320, GOF mutations, CRISPR/Cas9 KO, H460, cobalamin, ouabain, non-small cell lung cancer.

Acknowledgments

Above all, I would like to acknowledge, with deepest gratitude, Professor Dr. Lezina for her invaluable mentorship, continuous encouragement, and expert guidance throughout my research work. She has provided me with suggestions and constructive feedback at each step of the research. Furthermore, if I struggled, Professor Lezina would step in and show how it is done, sharing her vast research experience. It has been a true privilege to work under her supervision.

I further extend my profound gratitude to the members of our research team – Darkhan, Diana, Dana, Ainur, and Zakka – whose help and technical assistance, along with insightful discussions, greatly enriched my research experience. Their dedication, openness, and caring demeanor have truly made working in the laboratory much easier and more enjoyable.

My sincere thanks also go to the faculty members of NUSOM (Nazarbayev University School of Medicine) for providing an exceptional academic environment, which has greatly contributed to my scientific and personal development. My particular acknowledgments go to Professor Nikolai Barlev for his leadership, addressing lots of inquiries, sharing his experience with vast research expertise, and overall providing significant support throughout the studies. It is truly an honor to be under the mentorship of such a world-renowned scientist like him. Additionally, I would like to thank the MMM-2025 group for sharing so many pleasant and entertaining moments together during the course of the program.

Particular gratitude is extended to my dear parents and my sister, Tomiris Rakhimzhanova, who provided me with lots of love and motivation, who were guiding me and believing in me throughout this academic journey.

Table of contents

Table of Figures

Table of tables

1. Introduction

1.1 *TP53* in cancer – the guardian of the genome

The *TP53* gene is among the most thoroughly investigated genes in cancer biology because of its pivotal role in the onset and advancement of practically all human malignancies. (Kastenhuber & Lowe, 2017). Nearly four decades ago, p53 was mistakenly identified as an oncogene overexpressed in cancer. However, it is currently acknowledged as the most critical tumor suppressor and is often referred to as "the guardian of the genome" (Oren & Prives, 2024). By various mechanisms, it ensures that harmful "broken" cells are eliminated, allowing cells with intact genomes to maintain normal function. The active p53 promotes the synthesis of essential proteins such as cyclin-dependent kinase inhibitor p21, resulting in G1-S checkpoint arrest of the cell cycle. When DNA damage is irreparable, p53 initiates responsive mechanisms, including the activation of the *BAX* gene, which encodes a pro-apoptotic protein, ultimately resulting in cellular apoptosis or senescence. It additionally functions to suppress the *BCL2* anti-apoptotic gene and promotes the release of cytochrome c from the mitochondria. Cytochrome c stimulates caspases within the cell that are responsible for its eventual destruction (Joyce et al., 2023).

The role of *TP53* loss as a fundamental driver of human malignancies has been well established over the past four decades (Chen et al., 2022). Under cell exposure to environmental carcinogens, p53 functions to arrest the cell cycle and induce cell death of damaged cells to maintain the integrity of the genome. Premalignant cells are exposed to carcinogenic stimuli without a protective response when *TP53* is mutated. Consequently, the "genetically injured" cells proliferate and pick up further mutations, which eventually result in a tumor formation. This explains why *TP53* mutations are so frequently seen in cancer: only those malignant cells that have escaped p53's protective mode can survive the oncogenic stress.

In most cases, cancer cells carry mutations in one allele of *TP53*, and later in the progression of the disease, they tend to lose the last remaining wild-type *TP53* allele via loss of heterozygosity (LOH), with the effect being the expression of mutant p53 only (Sabapathy & Lane, 2017). In other cancers, TP53 mutations may act as the primary causal factor and occur very early in the oncogenic process. For example, *TP53* mutations in colorectal and triple-negative breast cancer occur with notable consistency (e.g., 50% - 90%) as early as the first or second stage of disease (Baker et al., 1990; Shah et al, 2012). But it is unknown if cancers with early TP53 mutations are more prone to LOH of the wild-type allele than cancers with *TP53* mutations that arise later in the development of the tumor. Regardless of the LOH status, *TP53* mutations are highly linked to poor responses to therapy and unfavorable prognosis across numerous cancer types (Sabapathy & Lane, 2017).

Typically, cancer cells have mutations in one *TP53* allele and, at a later stage in disease progression, frequently lose the last, wild-type *TP53* allele due to LOH, leading to the exclusive expression of mutant p53 (Sabapathy & Lane, 2017). Conversely, in some cancers, *TP53* mutations may serve as a primary causal factor and appear early in the oncogenic process. For instance, colorectal cancer and triple-negative breast cancer show a high prevalence of *TP53* mutations (ranging from 50% to 90%), even at early disease stages (Baker et al., 1990; Shah et al., 2012). But it is unknown if cancers with early TP53 mutations are more prone to LOH effect than cancers with *TP53* mutations that arise later in the development of the tumor. Regardless of the LOH status, *TP53* mutations are highly linked to poor responses to therapy and negative clinical outcomes in many types of cancers (Sabapathy & Lane, 2017).

1.2 Domain architecture of the p53 protein

Structurally, the p53 protein is organized into several functional domains (Figure 1): proline-rich domain, central DNA-binding domain (DBD) connected to tetramerization domain (OD), C-terminal regulatory domain (CTD), and N-terminal transactivation domain (TAD) (Wang et al., 2023). The TAD, comprising residues 1-61, interacts with regulatory proteins like MDM2, which leads to the ubiquitination of p53 in normal conditions (Joerger & Fersh., 2007). The PRD, spanning residues 64-92 seems to play a significant role in mediating apoptotic response in cancer cells (Baptiste et al., 2002) The central "core" DBD (residues 102-292) is crucial for recognizing and binding specific p53 response elements in DNA. According to Joerger & Fersht (2007) "It binds specifically to a double-stranded DNA consensus sequence consisting of two copies of a 10-base pair "half-site" motif, 5′-Pu*Pu*Pu*C*(A/T)*(T/A)*G*Py*Py*Py-3′ (where Pu represents A or G, and Py represents T or C), which are separated by up to 13 base pairs". The CTD at the extreme C terminus (residues 363-393) modulates p53 DNA-binding activity and stability through phosphorylation and acetylation sites. Furthermore, a highly conserved, leucine-rich nuclear export signal (NES) is located inside the tetramerization domain (residues 340–350), and a nuclear localization signal (NLS) spans the region between the core and tetramerization domains (residues 302–322).

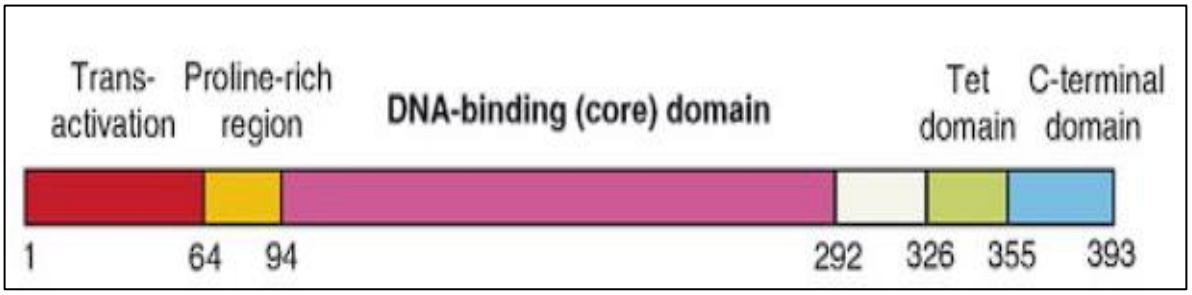

Figure 1. Schematic view of the domain structure of human p53.
"The main functional domains are the transactivation domain at the N-terminus, followed by a proline-rich region, the central DNA-binding core domain, the tetramerization domain, and the C-terminal negative regulatory domain"**.** *Adapted with the explanation from Joerger, A. C., & Fersht, A. R. (2007). "Structural biology of the tumor suppressor p53 and cancer-associated mutants."* Advances in Cancer Research, *97, 1-23.*

1.3 Prevalence of *TP53* missense mutations and their mechanism

Missense mutations predominate among *TP53* mutations in cancer, accounting for more than 75% of cases. These mutations usually result in a single amino acid substitution, which changes the architecture and activity of the p53 protein without causing it to be truncated. Most notably, the alterations often target DBD, thereby compromising its DNA-binding ability (Attardi & Boutelle, 2024). Common hotspots include residues R175, R248, R249, and R273 (Figure 1). DNA contact mutations, like R273H and R248Q, directly compromise p53's DNA-binding capacity, making it unable to bind to its downstream targets. Conversely, conformational changes like R175H and R249S disrupt p53's general structure and hence lower its functional capability (Zhang et al., 2020).

Nonsense and frameshift mutations generally produce premature stop codons, resulting in shortened and unstable proteins that are rapidly degraded through nonsense-mediated decay. These truncations, in effect, cause a complete loss of the protein's functionality, a phenomenon well-characterized in other tumor suppressors such as *RB1* and *APC* (Attardi & Boutelle, 2024). Yet, p53 does not entirely conform to this loss-driven narrative. Even in its truncated forms, certain

isoforms may retain fragments of their original capabilities, selectively preserving some functions while forfeiting others. For example, the p47 isoform, despite its lack of the transactivation domain (TAD), has demonstrated the capacity to trigger a particular set of apoptotic genes, as illustrated by Tong et al. (2021). This process is mediated by K382 acetylation, which uniquely enables p47 to recruit critical cofactors, thereby facilitating targeted gene activation in ways that diverge from the canonical functions of full-length p53.

1.4 Gain-of-Function mutations in p53 and the "Rainbow of Mutants"

The clear preference for missense mutations in *TP53* points to a much more complex strategic selection process at work. These mutations often maintain the full-length p53 protein, albeit with structural changes, hinting at a possible GOF effect. GOF mutant p53, along with the loss of its tumor-suppressive function, also acquires new tumorigenic capabilities, which include promoting cell proliferation, survival, invasion, and drug insusceptibility (Alvarado-Ortiz et al., 2021; Stein et al., 2019). Varda Rotter with colleagues reported one of the first examples of this phenomenon in TP53-deficient cells transfected with an overexpression vector for mutant p53 (Wolf et al. 1985). They showed that *TP53*-null cells overexpressing mutant p53 formed lethal tumors in mice, unlike *TP53*-null cells, which only developed regressing local tumors. Subsequently, mutant's p53 GOF activity was also observed in a great number of both in vitro (Eliyahu et al., 1985; Shaulsky et al 1991; Dittmer et al. 1993), and in vivo studies with mutp53 knock-in mice models (Lang et al., 2004; Olive et al. 2004).

To describe the variety of GOF activities exhibited by different p53 mutations Sapabathy and Lane (2017) introduced the term "rainbow of mutants" (Figure 2). According to their review, these p53 mutants, form a spectrum that differs widely in their GOF effects on tumor progression, depending on the nature and position of the mutation within p53's structural domains. Mechanics-wise, mutant p53 with GOF properties has been shown to enhance cell proliferation by interacting with various transcription factors and co-regulators differently from original binding sites (Sabapathy & Lane 2017). For instance, the mentioned R273H mutant p53 forms complexes with NF-Y & NF-kB and the co-activator p300 to activate cyclins A and B, as well as CDK1, driving cell progression. Similarly, mutant p53 collaborates with YAP in the same manner (Zhang et al. 2020). Compared to p53-null mice, R172H and R270H mutant p53 knock-in mice models generate more aggressive and metastatic cancers (Lang et al., 2004). These mutants promote epithelial-mesenchymal transition (EMT) by repressing *mIR-130b*, which upregulates EMT-related factors like *ZEB*1, and by interacting with p63 to activate *TGF-β* signaling.

It has been shown that the R248W and R273H p53 mutants attach to the nuclease Mre11, which inhibits the formation of the MRN complex at double-stranded DNA break sites, hence preventing ATM activation (Liu et al., 2009). Similarly, R175H and A193T mutations prevent DNA repair by attaching to E2F4, a protein that suppresses the transcription of critical repair genes, including *BRCA1* and *RAD17*. This interference damages DNA repair systems and contributes to genomic instability (Valenti et al., 2015). Additionally, R175H, 248Q, and R273H *TP53* mutations enhance glucose absorption and glycolysis, which dysregulate metabolism. By activating RhoA and crucial glycolytic enzymes such as hexokinase II, they cause the Warburg effect in cancer cells (Zhang et al. 2014).

Moreover, mutant p53 actively promotes pathways that increase tumor resistance to several drugs and chemotherapy therapies. One important strategy for reducing the intracellular accumulation of chemotherapeutic drugs is the upregulation of ATP-binding cassette (ABC) transporters, including *ABCB1* and *ABCG2*, which promote drug efflux. Additionally, mutant p53 lowers autophagy and apoptosis and promotes drug resistance by blocking the transcriptional

activity of p63 and p73. This further decreases chemoresistance and therapeutic efficacy (Zhang et al. 2020).

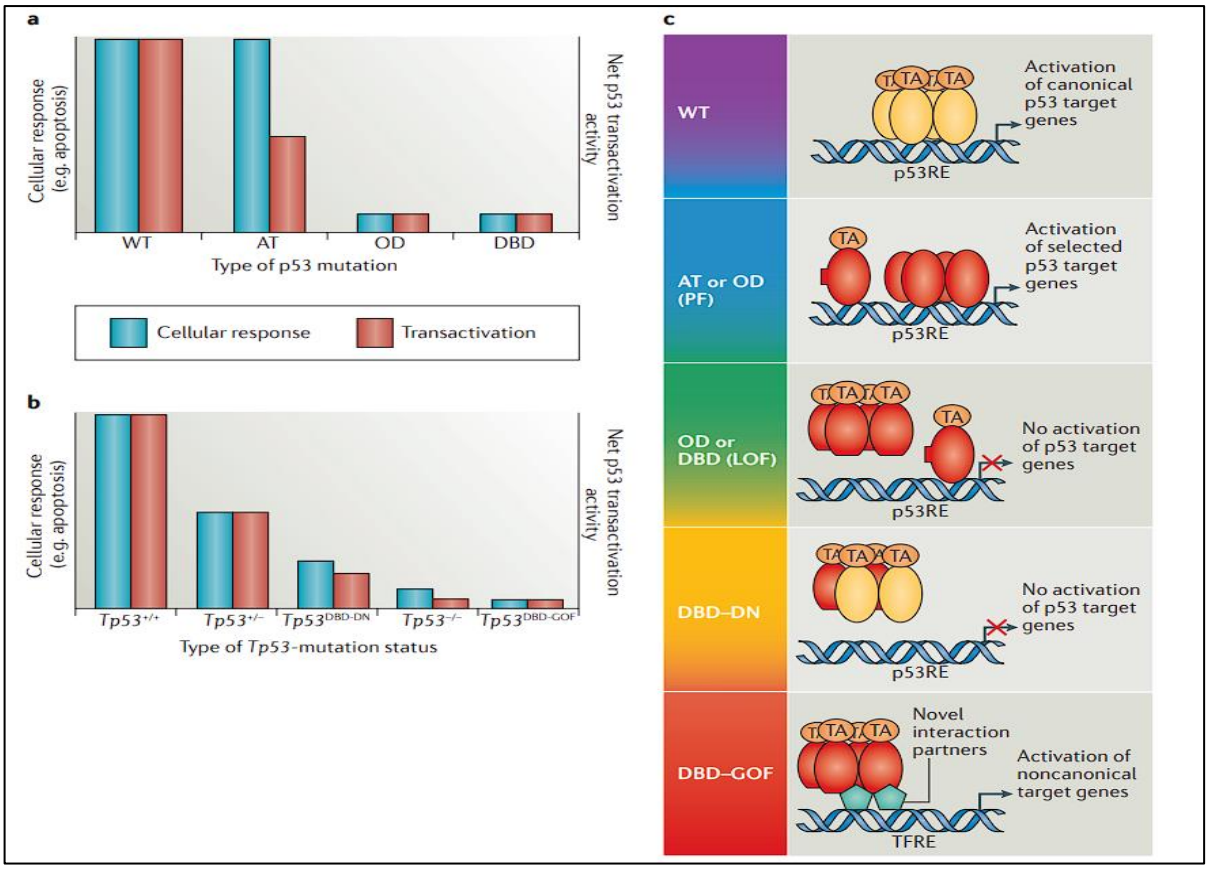

Figure 2. Rainbow of p53 mutants.
(A) The overall functional patterns of several p53 mutant categories are displayed in this panel. Red bars indicate the ability to induce transcription of typical p53 target genes, while blue bars indicate p53-dependent responses like cell-cycle arrest or apoptosis. Mutations within the amino-terminal AT domain tend to cause partial reductions in transcriptional function but still largely support p53-mediated cellular effects. In contrast, mutations within the DBD generally result in complete LOF, while mutations in the oligomerization domain OD also typically lead to LOF, though some may retain residual activity.

(B) This panel shows the behavior of DBD mutant p53 under genotoxic stress, specifically its GOF and dominant-negative DN characteristics, for both null (TP53−/−) and heterozygous (TP53+/−) genetic backgrounds. DBD mutants suppress the expression of p53 target genes, producing DN effects when co-expressed with wild-type p53. Certain DBD mutants acquire new oncogenic functions in p53-null environments, which encourage non-canonical cellular activities. The DN or GOF activities of AT or OD mutants in heterozygous states are still poorly understood, and the GOF phenotypes of these mutants are still up for debate.

(C) This schematic, known as the "rainbow of p53 mutants," classifies the distinct mutant forms based on their capacity for transactivation in p53-deficient environments. Wild-type p53 monomers are illustrated in yellow, whereas mutant p53 monomers are depicted in red. This summary emphasizes how p53 mutant classes differ in activating canonical versus non-canonical target genes.

Adapted from Sabapathy, K., & Lane, D. P. (2017). "Therapeutic targeting of p53: all mutants are equal, but some mutants are more equal than others." Nature Reviews Clinical Oncology, 15(1), 13–30.

These insights suggest that the high frequency of missense mutations in *TP53* is not coincidental but represents a selective advantage that allows tumors to co-opt mutant p53 for oncogenic purposes. This multifaceted "rainbow of mutants" presents both a challenge and an opportunity in cancer therapy. The broad variability of GOF activities underscores the need for therapeutic strategies tailored to specific p53 mutations. For instance, targeting mutant p53 stabilization pathways or inhibiting specific downstream interactions could mitigate GOF effects while sparing the wild-type-like properties retained in certain mutants (Stein et al., 2019).

1.5 CD320 and its role in cellular cobalamin uptake

CD320, often referred to as the transcobalamin receptor (TCblR), is a cell-surface receptor critical for the cellular uptake of cobalamin (vitamin B12) via binding to the cobalamin-transcobalamin (TC) complex (Alam et al. 2016). This protein, encoded by the *CD320* gene, belongs to the low-density lipoprotein receptor (LDLR) family and features its own distinct structural toolkit critical for cobalamin transport into cells (Figure 3). The receptor comprises an N-terminal extracellular domain containing two LDLR type A domains, LDLR-A1 and LDLR-A2, separated by an epidermal growth factor (EGF)-like domain, which enhances stability and facilitates ligand binding selectivity. Within each LDLR-A domain resides an internal calcium-binding site, a structural unit that tightens CD320's grip on its ligand, ultimately forming with other domains a high-affinity binding site for holo-TC. The transmembrane domain anchors CD320 with the plasma membrane, while a cytoplasmic tail contains an internalization motif essential for the cellular uptake of the receptor-ligand complex through clathrin-mediated endocytosis (Gick et al., 2020).

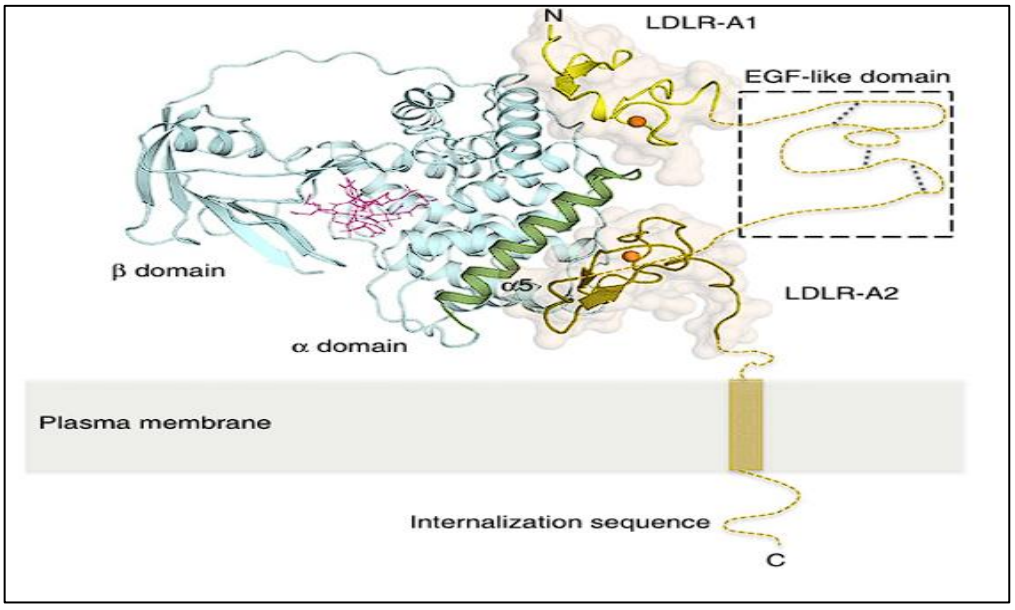

Figure 3. TC-CD320 complex.
"Overall structure of TC-CD320 complex showing TC (cyan) and LDLR-A1 and LDLR-A2 of CD320 (yellow and gold, respectively). The likely position of the EGF-like module (boxed) bridging the two LDLR-A domains is shown schematically. The transmembrane domain (yellow cylinder) and internalization motif of CD320 are shown in 2D format. Orange spheres represent bound Ca2 ions. Bound Cbl, sandwiched between the a and b domains of TC, is shown in pink and TC helix a5 is colored green". *Adapted with exact explanation from Alam et al., 2016. "Structural Basis of Transcobalamin Recognition by Human CD320 Receptor." Nature Communications, 7, Article 12100.*

Upon binding to holo-TC, CD320 undergoes conformational changes that trigger its internalization into the cell via clathrin-coated pits. Inside the cell, the receptor-ligand complex is trafficked to lysosomes, where holo-TC is degraded, releasing free cobalamin into the lysosomal lumen. This process enables vitamin B12 to exit the lysosome and participate as a cofactor in key cellular processes, such as methionine synthesis and fatty acid metabolism (Figure 4), which are essential for DNA synthesis and cellular proliferation. Unlike other receptors within the LDLR family, CD320 does not recycle back to the plasma membrane following internalization; instead, it undergoes lysosomal degradation along with its ligand, necessitating the synthesis of new receptors to replenish CD320 on the cell surface. This regulation tightly links CD320 expression to the cell cycle, with peak receptor levels observed during the S phase in rapidly dividing cells, and diminished expression in quiescent or differentiated cells (Gick et al., 2020).

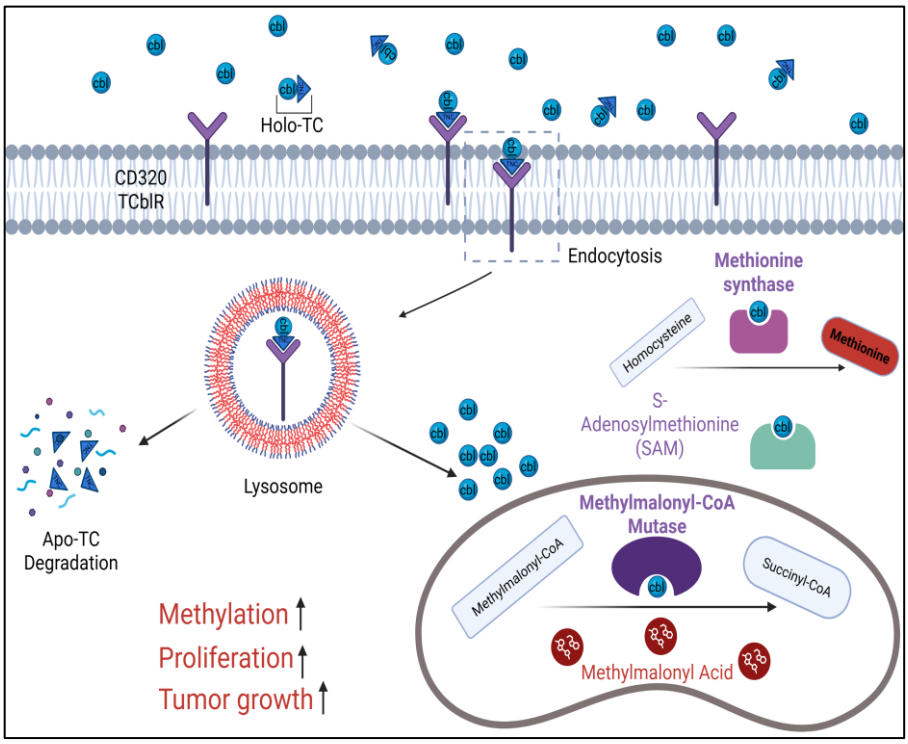

Figure 4. CD320's role in cobalamin uptake.
This diagram demonstrates how cells take up cobalamin–transcobalamin (Cbl–TC) complex in a receptor-dependent mode of endocytosis mediated by the CD320 (TCbIR) receptor. After internalization, the complex is trafficked to lysosomes, where transcobalamin is degraded, releasing free cobalamin. The freed cobalamin then acts as a cofactor for methionine synthase, which converts homocysteine to methionine, and for S-adenosylmethionine synthase (SAMS), which generates S-adenosylmethionine (SAM), a major methyl donor in epigenetic regulations. Additionally, cobalamin serves as a cofactor for methylmalonyl-CoA mutase, which in the catalytic process produces methylmalonic acid – an oncometabolite. Overexpression of CD320 enhances cobalamin uptake, fueling increased methylation reactions, cellular proliferation, and tumor growth. *Created in https://BioRender.com*

2. Hypothesis & aims

2.1 CD320 in cancer

The increased metabolic and proliferative demands in cancer often lead to higher CD320 expression. Lung, breast, and colorectal cancer are among those that have shown this elevation of transcobalamin receptor. Studies demonstrate that elevated CD320 levels correlate with aggressive cancer phenotypes and poor prognoses, since enhanced vitamin B12 absorption enables cancer cells to meet their higher biosynthetic requirements (Lai et al., 2011). Moreover, CD320's restricted ligand specificity, since it only binds holo-transcobalamin and no other cobalamin-binding proteins such as haptocorrin, renders it a notable marker and a potential target for tumor-specific treatment (Gick et al., 2020). Quadros and Sequiera (2013) also suggest that the receptor is well designed for customized drug delivery methods based on its structural and functional attributes. This facilitates the precise selective destruction of cancer cells that overexpress CD320, while safeguarding normal cells, by the use of anti-CD320 monoclonal antibodies or nanobodies coupled with cytotoxic agents (Quadros & Sequeira, 2013).

2.2 Unraveling new paths: The influence of GOF p53 on CD320 expression

Although the functions of CD320 in cobalamin absorption and p53 in tumor suppression and progression are well-documented, direct evidence linking CD32O and p53 in cancer literature remains scarce. While mutant p53's GOF activities contribute to altered cellular processes, including the described enhanced metabolism, proliferation, and drug resistance, it remains uncertain whether these effects extend to the control of CD320 expression. Nevertheless, preliminary data by Dr. Lezina show that at least a subset of GOF p53 mutants actively promote tumors by inducing expression of CD320, a receptor associated with enhanced vitamin B12 absorption and stimulating the growth of malignant cells.

In light of these challenges and emerging unpublished data from Dr. Lezina research, we will examine how oncogenic gain-of-function p53 mutants that frequently power the aggressive phenotype of NSLC also regulate the transcriptional and translational output of CD320. Establishing this connection will enhance comprehension of the role of GOF p53 mutations in metabolic reprogramming inside cancer cells, identifying CD320 as a possible downstream target of mutant p53 in NSCLC.

Thus, we hypothesize that CD320 is a bona fide target of mutant p53 in non-small cell lung cancer.

2.3 Aims & objectives

In the study, we investigate the possible ways through which mutant p53 regulates CD320 expression, and thus the potential of CD320 as a therapeutic target to improve the responsiveness of non-small lung cancers harboring GOF p53 mutants to treatment.

To explore this hypothesis, we will employ CRISPR/Cas9-mediated KO of the CD320 gene in NSCLC cell lines with different p53 status. To achieve this, we will employ the following steps:

1. Design and generate plasmid constructs expressing sgRNA for CD320 KO;
2. Knock out the CD320 gene in the H460 & H1975 cell lines using endonuclease Cas9 and the generated sgRNA constructs;
3. Analyze the impact of CD320 KO on the cell proliferation rates in cell lines with varying TP53 status.

3. Materials & methods

3.1 Materials

3.1.1 Chemicals & reagents

Presented below is the list of the chemicals and reagents applied in the research with the corresponding catalogue number and manufacturer's name.

- Agarose, #8100.00 (Sigma-Aldrich)
- Acetic acid (Glacial), EMPARTA, K48810430 707 (Merck)
- Ampicillin 1g N1, N000068/02 (SYNTHESIS, JSC)
- Bacterial agar, #1800 (Sigma-Aldrich)
- Cutsmart buffer, #B6004S (New England Biolabs)
- DMEM + GlutaMax 500 mL, Ref 61965-026 (Gibco)
- DMEM, Low Glucose 500 mL, Ref 10-567-014 (Gibco)
- DMSO, #N8418 (Sigma-Aldrich)
- DNA marker Sky-High, #S-8000 (Biolabmix)
- Ethanol, 96% (Lab source)
- FBS (Fetal bovine serum) 10%, (Gibco)
- Gel loading dye Purple (6X), #B7024A (New England Biolabs)
- Hi-Di formamide, #4311320 (Thermo Fisher Scientific)
- Lipofectamine 2000, #11668019 (Thermo Fisher Scientific)
- Lysogeny broth, L3522 (Sigma-Aldrich)
- NEBuffer2.1, B6002SVIAL (New England Biolabs)
- Opti-MEM reduced medium 500 mL, #31985-070 (Gibco)
- Ouabain octahydrate, 4995 (Sigma-Aldrich)
- PBS tablets, Ref 18912-014 (Gibco)
- PenStrep, 100X 100mL, Ref 30-002-Cl (Corning)
- Sodium acetate (3M, pH 5.2), #SC119071172 (Evrogen)
- TriDye1kb Plus DNA Ladder, N3270S (New England Biolabs)
- Trypan Blue, T10282 (Invitrogen)
- Trypsin (Invitrogen)
- TrypLE express (Gibco)
- Tris base, Ref 10708976001 (Roche)

3.1.2 Primers

Presented below is the list of all primers used in the study with the corresponding name and sequence. Primers were synthesized in DNA-oligonucleotide synthesizer ASM-800 (Nazarbayev University, core facility).

- sgRNA1 F: 5' CACCGGTTGGAGCGTGGCGAACAG 3'
- sgRNA1 R: 5' AAACCTGTTCGCCACGCTCCAACC 3'
- sgRNA2 F: 5' CACCGTGAGTGACGCCCCGCAGCG 3'
- sgRNA2 R: 5' AAACCGCTGCGGGGCGTCACTCAC 3'
- sgRNA3 F: 5' CACCGAGCGGCGGTTGGATGGCGC 3'
- sgRNA3 R: 5' AAACGCGCCATCCAACCGCCGCTC 3'

- sgRNA4 F: 5’ CACCGGTGGAAAGCGGGCTCGCGG 3’
- sgRNA4 R: 5’ AAACCCGCGAGCCCGCTTTCCACC 3’
- N1 Forward: 5’ GGGATAAGAGAGCGGTCTGG 3’
- N1 Reverse: 5’ GTGTCATGAACTGACGTGCG 3’
- U6 Sequencing primer: 5’-TGGACTATCATATGCTTACC-3’
- G3 Primer F: 5’ GACGAAACACCGAGTTCTGTAA 3’
- G3 Primer R: 5’ CAATACGCAAACCGCCTCTC 3’
- F8 Primer F: 5’ AAATAGGGGTTCCGCGCAC 3’
- R2 Primer R: 5’ GGTTTCGCCACCTCTGACTT 3’

3.1.3 Kits and Enzymes

Presented below is the list of all kits and enzymes used in the study with the corresponding catalogue number and manufacturer’s name.

- BigDye Terminator Cycle Sequencing Kit v3.1, #4337455 (Thermo Fisher Scientific)
- QIAquick PCR Purification Kit (50), Ref 28104 (Qiagen)
- QIAEX II Gel Extraction Kit (150), Ref 20021 (Qiagen)
- Evrogen Plasmid Miniprep Color, BC1215 (Evrogen)
- Evrogen MIDIPREP 3.0, BC224 (Evrogen)
- Phusion HF PCR MM, M0531S (New England Biolabs)
- Q-Load PCR Taq 2x MM, M0271L (New England Biolabs)
- BsaI-HFv2, #R3733 (New England Biolabs)
- HindIII-HF, #R3104 (New England Biolabs)
- T4 DNA ligase, #E320 (SibEnzyme)
- Proteinase K, #EO0491 (Thermo Fisher Scientific)
- NdeI, #R0111S (New England Biolabs)
- NotI, #R0189S (New England Biolabs)

3.1.4 Cell Lines and Bacteria

Presented below is the list of all cell lines and bacteria utilized in the study.

- H460, H1975 (Lab source)
- *E. coli* chemo-competent strain: *XL1*, *STBL*, *DH5α* (Lab source)

3.1.4 Plasmids

Presented below is the list of plasmids utilized in the study, including the corresponding plasmid number and the manufacturer’s name.

- ATP1A1_G3_Dual_sgRNA Plasmid, #173202 (Addgene)
- pMax_GFP Plasmid #177825 (Addgene)
- pRG2_GG_minus_1, Received from Dr. Guschin
- p3s-Cas9HC Plasmid, #43945 (Addgene)

3.1.5 Equipment

Presented below is the list of all equipment used in the study with the corresponding model number and manufacturer's name.

- Allegra X-12R centrifuge
- Allegra X-30R centrifuge
- Bio-Rad ChemiDoc MP imaging system
- Bio-Rad Mini-Sub Cell GT Cell
- Bio-Rad T100 Thermal Cycler
- DNA-oligonucleotide synthesizer ASM-800
- Eppendorf Centrifuge 5424
- Eppendorf Thermomixer C
- Esco class 2 biological safety cabinet
- Grant SUB Aqua Pro waterbath
- Binder CB-S CO2 Cell incubator
- Heratherm IGS400 incubator
- IKA KS4000 Control shaker
- Maestrogen UV transilluminator
- Mettler Toledo weighing scales
- NanoDrop 2000c Thermo Fisher Scientific spectrophotometer
- Sartorius water purification system
- SIGMA 1-14K centrifuge
- Stackable binder C170 REQ-53 cell incubator
- Waldner Scala bench mounted fume hood
- ZEISS Primovert Cell culture microscope

3.2 Methods

3.2.1 PCR settings

All PCR reactions were carried out in a T100 Bio-Rad Thermo Cycler. 2 different PCR kits were utilized throughout the study: Phusion HF PCR MM (M0531S, New England Biolabs) and Quick-Load PCR Taq 2x MM (M0271L, New England Biolabs). The volume of PCR mixture varied throughout the study, however the most used was 10µL volume with 5µL of the corresponding 2X master-mix, 1µL of 5 µM forward primer, 1µL of 5µM reverse primer, 1 µL of DNA (~50ng), and 2 µL of mill-Q water. Thermal cycling conditions were optimized depending on the master mix used (Table 1).

Table 1. PCR conditions used in the study.
All reactions were carried out in Bio-Rad T100 PCR thermo cycler PCR machine following protocols provided by New England Biolabs (n.d)

Step	Temperature, °C	Time
Phusion HF PCR MM, (M0531S, New England Biolabs)		
Initial Denaturation	98	30 seconds
30 cycles	98	5-10 seconds
	62	30 seconds
	72	15-30 seconds per kb
Final Extension	72	5 minutes
Q-Load PCR Taq 2x MM, (M0271L, New England Biolabs)		
Initial Denaturation	95	30 seconds
30 cycles	95	30 seconds
	62	40 seconds
	68	1 minute per kb
Final extension	68	5 minutes
Hold	4	Infinite

Agarose gel electrophoresis was performed on all PCR results to confirm successful amplification and validate the predicted fragment size.

3.2.2 Gel electrophoresis settings

Agarose gel electrophoresis was performed using a Bio-Rad Mini-Sub GT Cell connected to a PowerPac power supply, operated at 80 – 120 V. Gels were prepared with agarose dissolved in 1× TAE buffer, and stained with 5 µL of ethidium bromide per 100 mL of gel solution. The agarose concentration was adjusted based on the size of the DNA fragment being analyzed: 1% for plasmid DNA (~2.5 – 3.4 kb), 1.3–1.5% for PCR amplicons larger than 500 bp, and 2% for fragments smaller than 500 bp. 1 x TAE was used as a running buffer, and additionally, 2 µL of ethidium bromide was added to the buffer after running the gel for 10-15 minutes.

The electrophoresed gels were visualized using a Bio-Rad ChemiDoc MP Imaging System under ethidium bromide settings with the auto-rapid exposure mode. In addition, a Maestrogen UV transilluminator was employed as a supplementary tool to confirm the visibility and integrity of the DNA bands. To confirm amplicon size, the TriDye 1 kb Plus DNA Ladder (N3270S, New England Biolabs) was used for PCR product analysis, while the Sky-High DNA Ladder (S-8000, Biolabmix) was utilized for plasmid verification.

3.2.3 CRISPR/Cas9 sgRNA design

For CD320 KO, it was decided to use CRISPR/Cas9 approach, based on the use of sgRNA, complementary to the target region, and Cas9 protein (PAM sequence is –NGG–), which ultimately establishes 2 cuts in the target gene. This region is then proceeded by NHEJ (for KO purposes, creating a frameshift deletion in the gene, making an incomplete protein.

For transfection, 4 pair of sgRNAs targeting exon 1 of CD320 gene were obtained via CHOP-CHOP v3 web toolbox (https://chopchop.cbu.uib.no/; Labun et al., 2019). Every sgRNA was synthesized using the following general structure: top strand oligonucleotide with a 5' CACC overhang followed by the 20-nucleotide target sequence; and bottom strand with a 5' AAAC overhang followed by the reverse complement of the 20-nucleotide target sequence. This structure ensured proper ligation into the pRG2_GG_minus1 cloning vector, digested by BsaI enzyme. Additionally, the first nucleotide of the gRNA was substituted with a guanine base (G), as this is the preferred transcription initiation site for the human U6 promoter. The total yield of generated sgRNA can be seen in the table below (Table 2).

Table 2. Sequence of the sgRNA against CD320KO.
Produced by CHOP-CHOP web toolbox for CRISPR/Cas9 mediated KO of the CD320 gene. (https://chopchop.cbu.uib.no/)

№	Name	Sequence, 5' – 3'		Coordinates on the gene (CD320), start – end
1	sgRNA1_CD320_KO	F	CACCGGTTGGAGCGTGGCGAACAG	8308245 – 8308265
		R	AAACCTGTTCGCCACGCTCCAACC	
2	sgRNA2_CD320_KO	F	CACCGTGAGTGACGCCCCGCAGCG	8308126 – 8308148
		R	AAACCGCTGCGGGGCGTCACTCAC	
3	sgRNA3_CD320_KO	F	CACCGAGCGGCGGTTGGATGGCGC	8308266 – 8308286
		R	AAACGCGCCATCCAACCGCCGCTC	
4	sgRNA4_CD320_KO	F	CACCGGTGGAAAGCGGGCTCGCGG	8308171 – 8308191
		R	AAACCCGCGAGCCCGCTTTCCACC	

An overview of the 6 possible combinations of sgRNAs used for targeting exon 1 of the CD320 gene, along with the corresponding deletion sizes and their compatibility with the reading frame (multiplicity of three), is presented in Table 3.

Table 3. Characteristics of sgRNA combinations.
Deletion size (in base pairs) and whether the deletion preserves the reading frame.

	Combinations of sgRNAs					
	1+2	1+3	1+4	2+3	2+4	3+4
Size of deletion, bp	139	41	94	160	65	115
Multiplicity of three	No	No	No	No	No	No

3.2.4 Primer design

Aside from sgRNA oligonucleotides, primers used in the study are presented in table 4. All primers were generated via Primer-BLAST webtool (https://www.ncbi.nlm.nih.gov/tools/primer-

blast/) using optimal conditions provided by the NCBI primer-designing guidelines (National Center for Biotechnology Information [NCBI], 2025).

Table 4. List of the main analytical primer used in the study with the sequence and coordinates on the target.

№	Primer label	Sequence, 5' – 3'	Target	Purpose	Amplicon size, bp	Coordinates on the target DNA start – end
1	U6, Fw	TGGACTATCATATGCTTACC	U6 promoter	Sequencing sgRNA for CD320 Knock-out	–	170 – 189
2	pRG2_F8, Fw	AAATAGGGGTTCCGCGCAC	pRG2_GG_minus plasmid		1497	3076 – 3094
3	pRG2_R2, Rv	GGTTTCGCCACCTCTGACTT				1415 – 1434
4	CD320_KO_N1, Fw	GGGATAAGAGAGCGGTCTGG	CD320	Confirming CD320 deletion	304	118 – 137
5	CD320_KO_N1, Rv	GTGTCATGAACTGACGTGCG				402 – 421
6	ATP1A1_G3, Fw	GACGAAACACCGAGTTCTGTAA	ATPA1_G3 plasmid	Sequencing sgRNA, targeting ATPA1	347	700 – 721
7	ATP1A1_G3, Rv	CAATACGCAAACCGCCTCTC				1027 – 1046

3.2.5 Vector digestion/ligation

Obtained sgRNA oligonucleotide pairs had been annealed before proceeding with vector cloning. Briefly, 25 µL mixture, consisted of 100pMol/µL of each complementary sgRNA and 1X NEBuffer2.1, (cat #B6002SVIAL, New England Biolabs) was subjected for annealing in T100 thermocycler (Bio-rad) following these parameters: [+95 °C 3 min.; +95 °C to +85 °C in - 2 °C/sec. increment; +85 °C to +25 °C in - 0.1 °C/sec; hold at +4 °C].

Simultaneously, 2µg of pRG2_gg2_minus1 plasmid was digested with the BsaI-HFv2 (cat #R3733, New England Biolabs) and HindIII-HF (cat #R3104, New England Biolabs) enzymes in accordance to manufacturer's provided protocol. After incubation with enzymes in thermomixer C at 37°C for 30 minutes, subsequent inactivation at 60°C for 15 minutes, cut plasmids had been ran on the 1% gel at 80V for 30 minutes in 1X TAE buffer. Additionally, native pRG2_gg_minus1 plasmid cut by BsaI only, and positively digested pRG2 had been also used to control digestion. The section of the gel with the band, which corresponded to the size of digested plasmid (around 2,5kb) had been cut out under UV inspection with scalpel and purified using QIAEX II Gel Extraction Kit (cat #20021, Qiagen) according to the manufacturer's provided guidelines. Ultimately, the concentration of the yielded plasmid was checked via Thermo Fisher Scientific Nanodrop 2000c.

After obtaining both annealed sgRNA and digested pRG2_gg_minus1 plasmid, ligation reaction was carried out in 20µL mixture, consisted of 3µL of the digested plasmid (21.1ng/µL), 1µL of annealed sgRNA(100pMol/µL), 2µL of 10X ligation-buffer, 1µL of T4 DNA ligase (cat #E320, SibEnzyme) and 13µL Milli-q water. The ligation mixture was then incubated overnight at 12°C in Eppendorf C thermocycler.

3.2.6 Bacterial transformation

Bacterial transformations were performed in chemically-competent *Escherichia coli* strains with the sgRNA constructs in an ampicillin resistant pRG2_GG_minus1 plasmid backbone. Bacterial transformations were conducted using both *XL1-Blue* and *Stbl3* competent cells, however, none produced colony formation through subsequent transformations. That suggested that both strains had poor transformation efficiency under the conditions employed. In contrast, only *DH5α* competent cells formed sufficient colonies for subsequent experiments.

Both *DH5α* cryovials and protocol for transformation were provided by Yergali Bexeitov. In short, for each of the tubes, 50 µL of thawed competent cells were aliquoted into pre-chilled on ice 1.5 mL microcentrifuge tubes. Plasmid DNA (2 ng) was then added to each aliquoted competent cell, and mixed by flicking the tubes five times. The competent cells were transferred to ice and incubated for 30 minutes before a heat shock at 42 °C for 1 minute. After heat shock, the competent cells were transferred to ice for 5 minutes and recovered in 900 µL of LB broth (Luria-Bertani, Miller (cat #L3522, Sigma-Aldrich) medium containing per liter: 5 g of Yeast extract, 10 g of NaCl and Tryptone respectively; pH ~ 7.00) and incubated for 40 minutes in Eppendorf Thermomixer C at 37 °C, 300 RPM.

The transformed cultures were then plated out on Petri dishes with LB agar (LB with addition of 15g of bacterial agar (cat #1800, Sigma-Aldrich)) with 100 µg/mL ampicillin for incubation in Heratherm IGS400 incubator at 37 °C for overnight growth. To encourage dense colony growth, the transformation suspension from the cells was plated out using a range of volume (25, 50, 100 and 200 µL). Additionally, 3 controls were implemented: DH5a transformed with an unligated plasmid; DH5a transformed with native pRG2_GG_minus1 plasmid; and plate with LB agar and ampicillin (100µg/mL) for controlling antibiotic efficiency.

3.2.7 Plasmid DNA extraction

SgRNA-carrying plasmids were extracted from bacteria using two methods: an initial simple heating method for PCR screening of positive colonies, and plasmid purification using the MIDIPREP 3.0 kit (cat #BC224, Evrogen).

For the simple extraction, 2mL of overnight liquid cultured bacteria was placed into a 2 mL centrifuge tube and spun down at 5000RPM for 10 minutes. After discarding supernatant, the bacteria pellet was then resuspended with 100µL milli-q water and incubated in thermocycler at 100°C for 10 minutes. Afterwards, by adding additionally 900 µL and making sure that the suspension is homogenous, the tube was spun down again at 12000RPM for 10 minutes. After centrifugation, supernatant had been transferred to a labeled sterile 2 mL Eppendorf tube. For PCR screening, 3µL of extracted plasmid had proven to be sufficient.

Prior to midiprep extraction, 1 positive DH5a colony with corresponding sgRNA vector was inoculated in 1L shake flask with 100mL LB broth (100µg/ml of ampicillin) for 18h at 37°C, 250RPM on IKA KS4000 Control shaker. Additionally, 1ml of 2 confirmed colonies from each

sgRNA were frozen in glycerol at -80°C freezer. Then, to obtain high-copy plasmid yield midiprep extraction had been done following the manufacturer's provided guide.

3.2.8 Sequencing

Sequencing of the constructed plasmids were performed using in ABI 3500 genetic DNA Analyzer (Applied Biosystems). Samples for sequencing were prepared in the following way:

Firstly, plasmids were amplified using Quick-Load Taq2X MM in 10 µL reaction volume, by 5µM of corresponding primers (F8 + R2 for pRG2_GG_minus1, G3 forward + reverse for G3, G4 forward + reverse for G4). Products were then verified by running on 1% gel electrophoresis at 80V for 40 minutes. If verified, products were purified using the QIAquick PCR purification Kit (cat #28104, Qiagen) and quantified using a Thermo Fisher Scientific NanoDrop 2000c.

Purified PCR products or plasmids (for direct sequencing) were subjected to a second PCR with BigDye Terminator Cycle Sequencing Kit v3.1(cat #4337455, Thermo Fisher Scientific) in Bio-Rad T100 Thermo Cycler. The reaction mixture consisted of 1 µL of 5µM one specific primer, 2µL of BigDye, 1µL of purified DNA(~8-10ng), and milli-q water. Thermal cycling conditions were as follows: 25 Cycles [95°C – 1 minute; 95 – 10 sec; 55 – 5 sec; 60 – 4 min], hold at 4°C.

Before analyzing, DNA products were precipitated. Briefly, 50µL of sodium acetate/ethanol solution (37.5 µL 3M sodium acetate, pH 4.6-5.2; 782.5µL 96% ethanol; 180 µL dH20) was added to each 10 µL product tube. After adding solution, samples were incubated at room temperature for 30 minutes, then centrifuged at 13,200 × g for 30 minutes at 4 °C. The supernatant was discarded, and 80 µL of 75% ethanol was added. After a second centrifugation step under the same conditions, the pellet was air-dried for approximately 30 minutes at room temperature. Finally, dried pellets were resuspended in 14 µL of Hi-Di formamide, thoroughly vortexed, and incubated at room temperature for 20 minutes. Samples were then denatured at 95 °C for 2 minutes, placed on ice for 5 minutes, and then passed for analyzing.

3.2.9 Cell culture

The H1975 cells (ATCC CRL-5908) were initially included in the early stages of the study, however, they were ultimately excluded from the experimental procedures due to practical limitations encountered during culturing, including slow proliferation rate, low survival and high sensitivity. Thus, the work will be mainly focused around H460 cell lineage.

The H460 cell line (ATCC HTB-177) originates from the pleural effusion of a male patient and represents a human non-small cell lung carcinoma cell line. These cells express epithelial morphology and contain wild type p53. The cells in laboratory were acquired from the American Type Culture Collection (ATCC) and stored in -80°C freezer.

Although RPMI-1640 is the recommended medium for culturing H460 cells, Dulbecco's Modified Eagle Medium (DMEM) with high glucose (4.5 g/L) and L-glutamine supplemented with 10% fetal bovine serum (FBS) and 2X Penicillin-Streptomycin (200 units of penicillin and 200 µg of streptomycin per mL) was used in the study. Cells routinely cultured in a «STACKABLE BINDER C170 REQ-53» incubator at 37°C with a 5% CO2. For routine passaging and pre-transfection conditions, cells were maintained in 10 cm culture plates with 10 mL of complete DMEM. Cells were either passaged or used for experimental procedures depending on their confluency, which was basically maintained below 90%.

A detailed summary of the plate formats used in this study, including the volumes of PBS for washing, trypsin for detachment, and complete medium per well, as well as the surface area of each plate type, is provided in the table below.

Table 5. Volumes of PBS, Trypsin, and Complete Medium (DMEM) used for different plate formats using Thermo Fisher Scientific guidelines (n.d).

Plate type	Surface area, cm^2	Medium volume per well, mL	Trypsin volume, µL	PBS washing volume, µL
15cm dish	~145	20	2000	5000
10cm dish	~55-60	10	1000	3000
6cm dish	~21-22	5	500	1500
6 well plate	~9.5 per well	2	300	1000
12 well plate	~3.8 per well	1	150	500
24 well plate	~1.9 per well	0.5	50	300
96 well plate	~0.3 per well	0.2	30	100

3.2.10 Cell seeding

The cell stock used in this study was provided from the frozen bank of the phD student Darkhan Issakhanov. The H460 containing cryovial was pre-warmed in the water bath at 37°C and then diluted in 10mL of complete DMEM in a sterile 15 mL conical tube. After gently swirling the tube, centrifugation at 300xg for 5 minutes was carried out at room temperature to pellet the cells. Once centrifuged, in order to remove DMSO and cell debris, the medium was carefully aspirated without disturbing the pellet and then resuspended in 5 mL and mixed until homogenous solution was formed. Resulting suspension was then transferred into 10cm plate with 5mL complete DMEM and incubated at 37 °C in a 5% CO_2 incubator.

3.2.11 Cell freezing

For the preparation of a custom frozen cell stock, 15 cm plates with 20 mL of complete DMEM were used for culturing the cells. Subsequently, they were cryopreserved upon reaching a confluency of at least 90%. The exhausted culture medium was aspirated under sterile conditions inside the BSL-2 Esco hood before washing the cells twice using 10 mL of phosphate-buffered saline (PBS). Afterward, cells were detached during a 2–3-minute incubation at 37°C with 5% CO2 using 2 mL of 0.05% Trypsin. The enzymatic activity was then neutralized by adding 8 mL of complete DMEM (1:4 ratio with trypsin). Resulting 10mL suspension was then transferred into a sterile 15 mL conical tube and centrifuged at 1000 RPM for 5 minutes. Afterwards, cells were resuspended in 1mL of freezing medium (10% DMSO and 90% complete DMEM). The final suspension was then thoroughly mixed and transferred into labeled cryovials (initials, cell line, the date and PI's name), which were gradually cooled to -80°C.

3.2.12 Cell transplantation

Transplantation of cells for transfection was carried out when 80% confluency was observed visually under the ZEISS Primovert microscope and by counting in Neubauer hemocytometer. After washing 10 cm plates twice with 5 mL PBS, treating with 1 mL of 0.05% trypsin and incubating for approximately 2-3 minutes at 37°C with 5% CO2, 4 mL of complete DMEM were added to make a suspension of cells for transplantation. Following this, only a calculated portion of the cell suspension was transferred to ensure that the well would reach 80–90% confluency the following day.

3.2.13 Cell counting

In order to precisely transfer exact number of cells for transfection (per protocol), cells were counted in Neubauer hemocytometer. As previously described, cells were harvested by incubating with 1mL 0.05% trypsin at 37°C in a 5% CO_2 incubator for 2–3 minutes after washing the plate twice with PBS. Additionally, cells were analyzed under the ZEISS Primovert microscope to ensure complete detachment from the plate surface. After neutralization of trypsin by adding 4mL of complete DMEM, the resulting cell suspension was centrifuged at 1000RPM for 5 minutes at room temperature. The supernatant was then carefully aspirated without the disturbance of pellet. The cell pellet itself was intensively resuspended in 1mL of complete cell culture medium to ensure a uniform cell suspension. From this, 10 µL of homogenized suspension was transferred into a sterile 1.5mL Eppendorf tube and mixed with 10 µL of 0.4% trypan blue. Lastly, a hemocytometer was filled with a 10-microliter sample of the stained cell mixture. Four corner squares' worth of cells were counted, and the formula below was used to get the total number of cells:

$$(a + b + c + d) / 4 \times 10^4 \times DF = \text{cells/mL}$$

Where a, b, c, and d stand for the cell counts in the corresponding four squares and DF – dilution factor (equal to 2 since cells were diluted in a 1:1 ratio with trypan blue).

3.2.14 Cell transfection

H460 cells were transfected in 12-well plate with 6 possible sgRNA combinations, and 3 controls (Figure 4). One day prior to transfection, cells were counted and 0.2 x 10^6 cells were seeded per well with 1 mL of complete DMEM. Since H460 doubling time approximates to 23 hours, after exact that time transfection was carried out with 0.4 x 10^6 cells in each well.

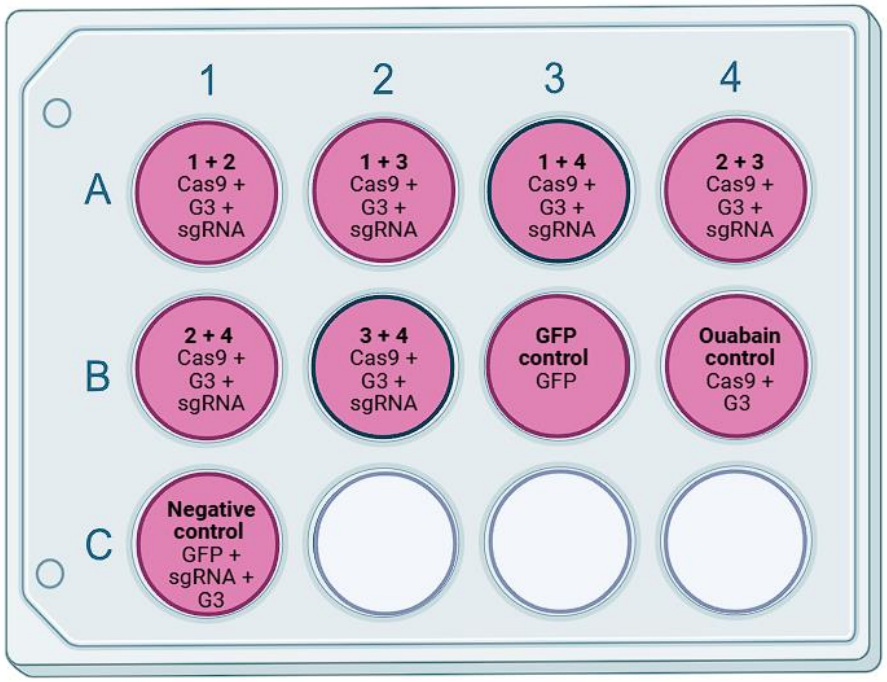

Figure 5. The scheme of H460 transfection for obtaining CD320 KO clones.
Wells with 6 possible combinations, GFP control, positive Ouabain control and Negative control are present along the plasmids that had been used. The ratio of plasmid for transfection is 70% cas9 + 20% of 2sgRNA + 10% G3. *Created in https://BioRender.com*

For transfection, total 2µg of plasmid DNA per well was used in complex with Lipofectamine2000. For studying samples, 1.5ng of p3s-Cas9HC (cat #43945, Addgene), 0.15ng of 2 sgRNA_pRG2 plasmids (in combination), along with 0.2ng of ATP1A1_G3_Dual_sgRNA plasmid (cat #173202, Addgene), and 15µL of Lipofectamine2000 (cat #11668019, Thermo Fisher Scientific) were diluted in 0.5 mL Opti-MEM (Minimal essential medium, cat #31985-070, Gibco). Afterwards, DNA-lipofectamine complex was formed upon vortexing on maximum speed for 5 seconds and incubating at room temperature for 10 minutes. For transfection control, 2ng of pMax_GFP plasmid (cat #177825, Addgene) was used. For ouabain selection control, p3s-Cas9HC and ATP1A1_G3_Dual_sgRNA plasmids were used in ratio 80% to 20% respectively. For negative control, pMax_GFP plasmid, 2 sgRNA_pRG2 plasmids (1+2 combination), and ATP1A1_G3_Dual_sgRNA plasmid were used in 7:2:1 ratio respectively.

Upon transfection, after aspirating the medium in the wells, the content was then changed with DNA-Lipofectamine complex (corresponding plasmids) in 0.5mL of Opti-MEM. Subsequently, cells had been left for 6 hours and lipofectamine medium was then substituted with regular culture medium. To obtain the highest level of modification/deletion the transfected cells were cultured for 2 days.

3.2.15 Ouabain selection

Ouabain is a plant-derived, highly toxic substance (inhibitor of Na^+/K^+-ATPase) used for selecting genetically modified H460 cells. ATP1A1_G3_Dual_sgRNA (G3) plasmid introduces a Q118R mutation in exon 4 of the ATP1A1 gene, which confers resistance to ouabain, allowing selective survival of edited cells during treatment.

Ouabain octahydrate stock solution (68.6 mM) was prepared by dissolving 50 mg of powder (cat# 4995, Sigma-Aldrich) in 1 mL of DMSO (cat #N8418, Sigma-Aldrich) and intermittent vortexing to ensure complete solubilization. Serial dilutions (1/10, 1/100, and 1/1000) were performed using DMSO, with vortexing at each step to maintain solution homogeneity.

After 48 hours of transfection, cells were split: 75% into treatment groups and 25% into control groups. Treatment cells were seeded into fresh plates and exposed to ouabain octahydrate, diluted in DMSO at three concentrations (0.05 µM, 0.2 µM, and 0.5 µM). Control cells were maintained without ouabain to assess baseline transfection and editing efficiency. Ouabain selection was carried out for 4 days, followed by culturing in normal medium for 5 additional days. Selection efficiency was monitored using control samples:

- Negative control (transfection efficiency): H460 cells transfected with GFP-only plasmid (pMax_GFP);
- Positive control (ouabain resistance): H460 cells transfected with p3s-Cas9HC and ATP1A1_G3;
- Negative control (selection specificity): H460 cells transfected with GFP plasmid, sgRNAs, and ATP1A1_G3 without Cas9 carrying plasmid.

Surviving cells from ouabain-treated groups were subjected to single-cell colony picking, while control cells were gathered to isolate genomic DNA and conduct PCR assays. Presented below is the overall scheme for selection (Figure 5).

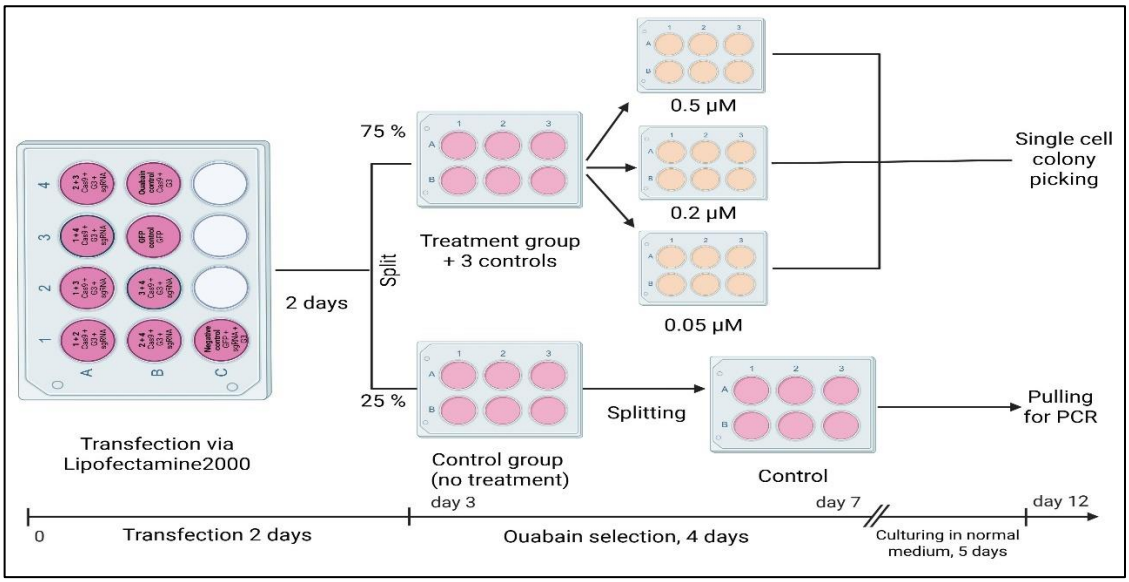

Figure 6. Ouabain selection workflow for H460 cell transfection.
H460 cells were transfected with Cas9, sgRNAs targeting CD320, and an ATP1A1_G3 plasmid using Lipofectamine 2000. After 2 days, cells were split into treatment (75%) and no treatment control (25%) groups. Treatment cells were exposed to different concentrations of ouabain octahydrate (0.05 µM, 0.2 µM, 0.5 µM) for 4 days to select resistant clones, followed by culturing in normal medium. Day 12 post transfection, single colonies were obtained for PCR analysis. At the same time, samples from no treatment group were collected by pulling for PCR. *Created in https://BioRender.com*

3.2.16 Single cell colony picking

Genome DNA was extracted from H460 ouabain positive selected colonies by following these steps:

Each colony had been observed under the microscope, and the approximate region where it resides was marked under the plate. Afterwards, 1 mL of DMEM complete medium was aliquoted into a sterile 1.5 mL Eppendorf tube. A 200µL tip with the media was then used to collect colonies by touching and aspirating with the bottom of the tip. Next, making sure that cell suspension is homogenous, 400µL was separated for DNA extraction, while 600 µL of the suspension had been seeded into a 24-well plate.

3.2.17 Genome DNA extraction

Extraction of genome DNA starts with aspirating the medium. Then, cells are collected from 6-well plate by incubating with 200µL of 0.05% Trypsin at 37°C, 5% CO2. After inactivating trypsin by 800 µL of complete DMEM, portion of cells are transferred into a sterile 1.5 mL Eppendorf tube. Next, the suspension is centrifuged at 500 x g in SIGMA 1-Mk centrifuge and resulting pellet is resuspended in 20µL of TrypLE Express 1X (#12604013, Gibco). To disturb the cells' membrane and get rid of cell proteins and debris, samples are then incubated with Proteinase K, (#EO0491, Thermo Fisher Scientific) in T100 thermocycler or Eppendorf C thermomixer, in the following way: initial membrane denaturation at 95°C – 5 minutes; adding 1 µL of 20 mg/mL Proteinase K and then incubation at 60°C – 30 minutes; enzyme inactivation at 95 – 5 minutes; hold at 4°C for 3 minutes. Extracted genome DNA is then subjected to a PCR on conditions, described above.

4. Results

4.1 Primer Validation for CD320 Knockout

To confirm the efficacy of the designed primers targeting the *CD320* gene, PCR reactions were performed on the genomic DNA from the T47D cell line using varying primer concentrations. Amplified products were analyzed by agarose gel electrophoresis (Figure 7). Successful amplification was observed at 0.66µM and 0.33 µM primer final concentration, indicated by the expected band size of 304 bp. Additionally, 62°C annealing temperature, provided by the primer-BLAST webtool had proven to be optimal as well.

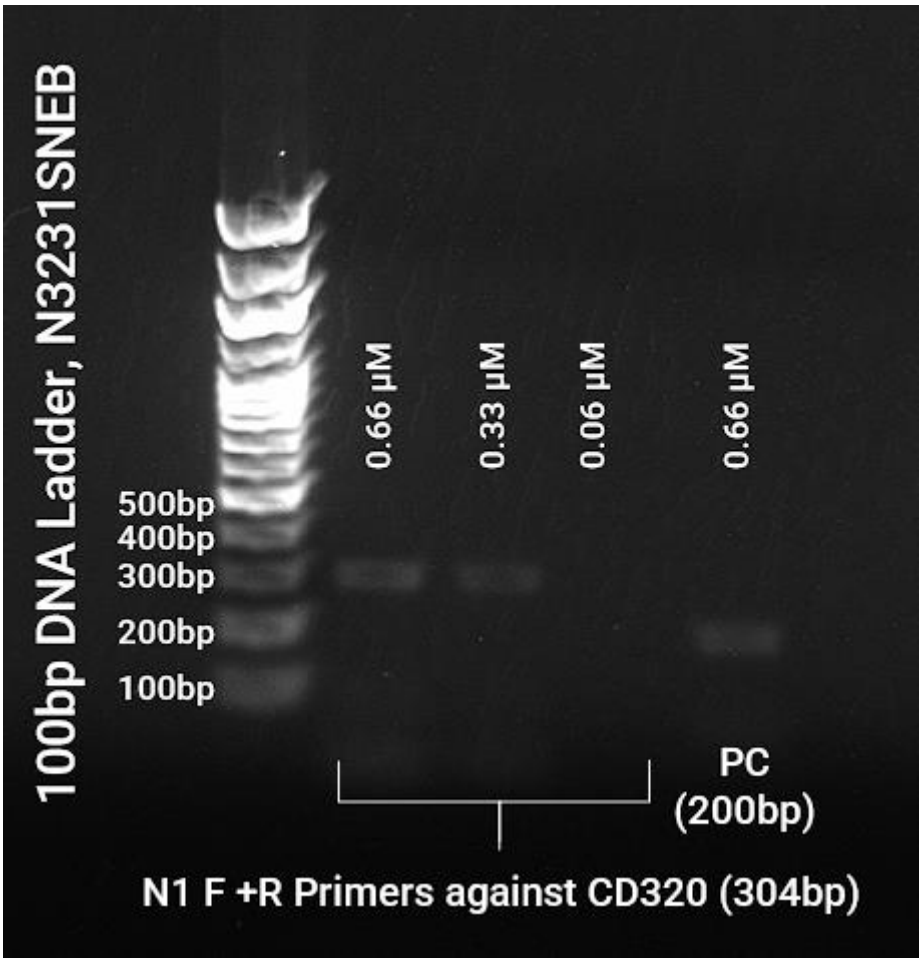

Figure 7. PCR analysis of N1_F and N1_R primer against CD320 gene in T47D extracted DNA.
PCR products were separated on a 1.3% agarose gel and visualized under UV light. The expected amplicon size is 304bp. 3 different primer concentrations were tested in 14µL reaction volume: 10µM, 5µM and 1 µM with 0.66µM, 0.33µM and 0.06µM final concentration respectively. Only 0.66µM and 0.33µM primers show expected band. 100bp DNA Ladder (N3231S, New England Biolabs) was used for size estimation.

4.2 Construction and Validation of sgRNA Expression Vector

4.2.1 Digestion of the pRG2_GG_minus1 plasmid

The pRG2_GG_minus1 was digested with BsaI to generate compatible ends for sgRNA cloning. pRG2 plasmid contains 2 sites for BsaI enzyme, which, when cut, produce a 676bp DNA fragment, which can be digested furtherly by HindIII, producing 172bp and 504bp. Since it is easier to control digestion with these fragments, pRG2 cut by both BsaI and HindIII simultaneously was used for digestion and further purification/extraction. Agarose gel electrophoresis confirmed successful double digestion, showing distinct bands at expected sizes (Figure 8).

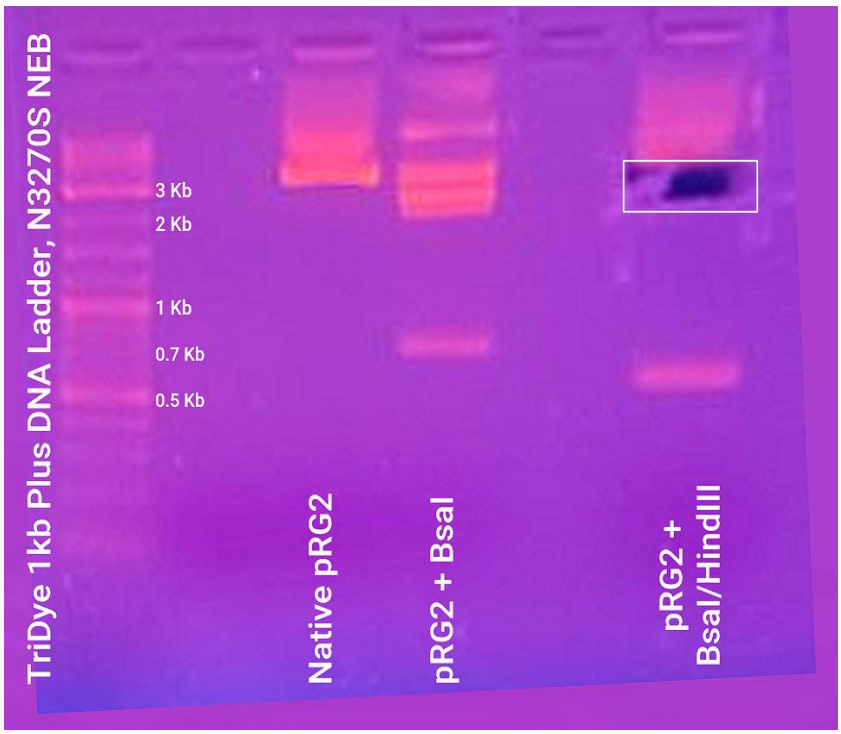

Figure 8. 1.5% agarose gel, visualized under UV transilluminator, showing digestion products.
Native pRG2 plasmid and pRG2 cut by BsaI were used as a control. Indicated in white rectangle is the region (~2.5kb) from pRG2 cut by BsaI/HindIII that was cut and furtherly purified for subsequent ligation. Additionally, byproducts of digestion (676bp and 504bp fragments) can be seen. TriDye 1kb Plus DNA Ladder (cat #N3270S, NEB) was used for size estimation.

4.2.2 Transformation and Colony Selection

Following ligation with the sgRNA insert, transformation into *E. coli* DH5α chemo-competent strain was performed. Colonies were successfully obtained on selective plates with 100µg/mL ampicillin (Figure 9).

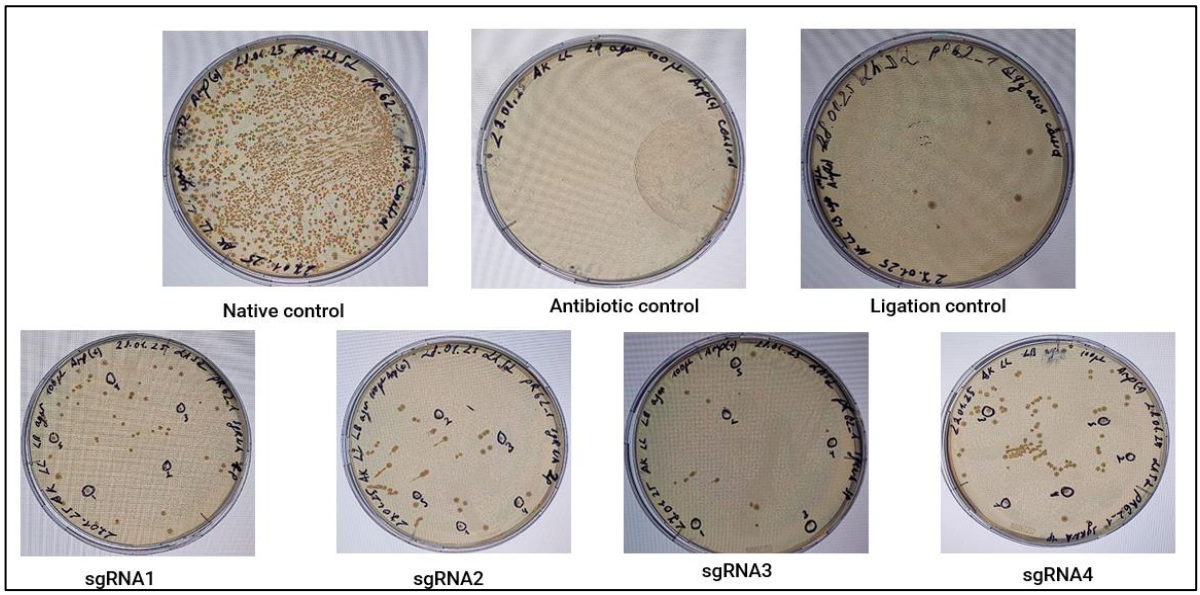

Figure 9. Selection of bacterial colonies after transformation with sgRNA constructs. Transformation efficiency was assessed by plating bacteria on antibiotic-containing LB agar (100µg/ml ampicillin). The control transformed with the undigested pRG2 plasmid showed dense bacterial growth, confirming viability. The antibiotic control (no plasmid, with 100µg/mL ampicillin) showed no growth, verifying antibiotic selection pressure. The ligation control (plasmid without sgRNA insert) resulted in few colonies, indicating low background ligation. Plates with sgRNA1, sgRNA2, sgRNA3, and sgRNA4 ligations showed the growth of positive colonies, out of which 5 were chosen for subsequent plasmid extraction.

Overall ligation efficiency was estimated by normalizing the ligation control (ligated pRG2 without sgRNA insertion) and counting the colonies in positive plates. The sample-to-control ratio for each plate is:

- 7 colonies in ligation control
- 52 colonies in sgRNA 1 – 1:7.4;
- 41 colonies in sgRNA 2 – 1:5.85;
- 17 colonies in sgRNA 3 – 1:2.42;
- 65 colonies in sgRNA 4 – 1:9.28.

Indicated below is the result of 18-hour inoculation of selected colonies:

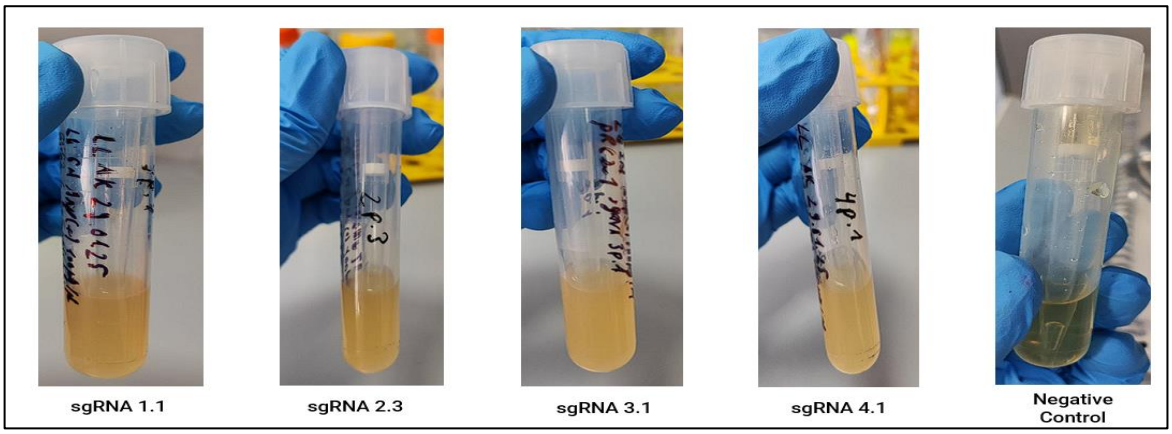

Figure 10. Liquid culture tubes with selected colonies after 18 hours inoculation. Compared to clear control (no bacteria), sample tubes became muddy, indicating successful culturing.

4.2.3 PCR Screening of Colonies

To verify the presence of sgRNA inserts in selected colonies, PCR screening was employed using F8 + sgRNA R primer combination, which yields approximately a 400bp product size. Since sgRNA R primer is specific to the sgRNA sequence, native pRG2 plasmid carrying colonies won't produce any band on the gel. Additionally, native control (primers F8 + R2 with 1497bp product) and positive control (positive sgRNA 4 colony primers F8 + sgRNA 4R, obtained from E. Zakka) were included in the screening. Ultimate results are shown in Figure 11.

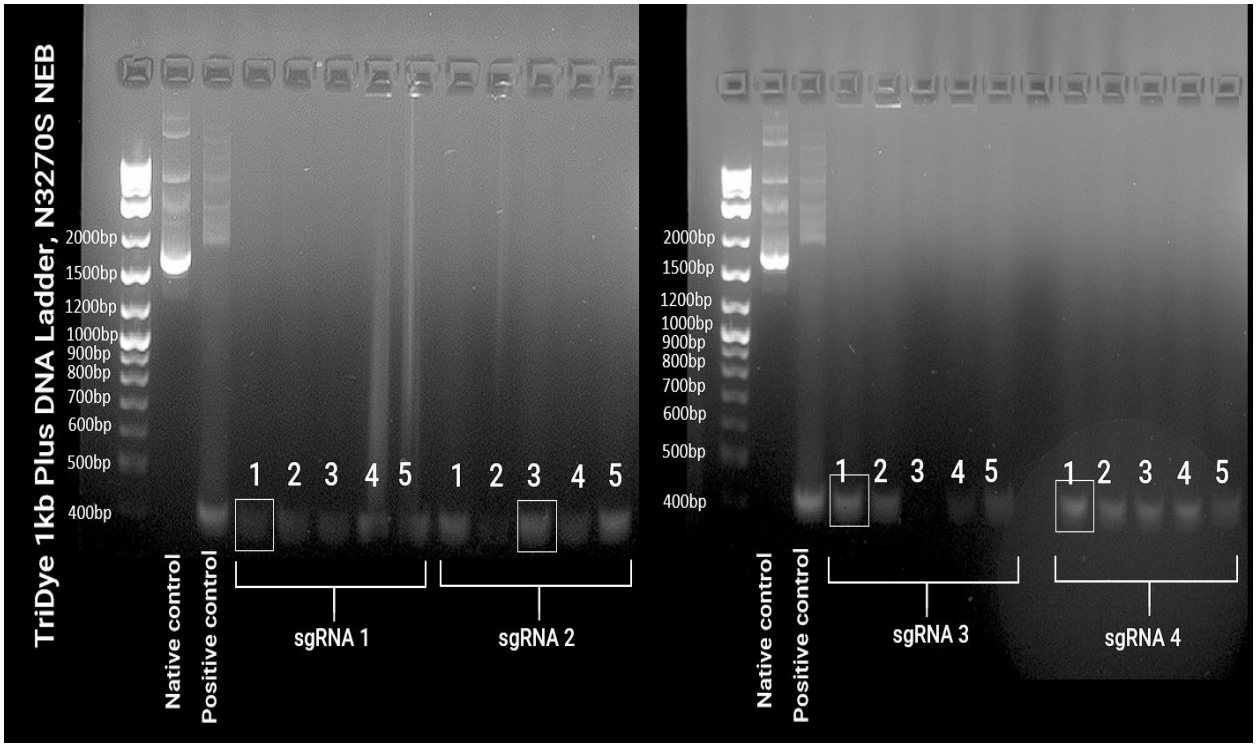

Figure 11. PCR screening for positive colonies, carrying corresponding sgRNA construct. PCR products were separated on a 2 1.3% agarose gels and visualized under UV light. Native control produces an expected ~1500bp band, indicating workable primers. For each sgRNA sample plate, 5 colonies were screened. Positive colonies produce a 400bp band. Indicated in a white rectangle is the colony, which was chosen for future plasmid extraction. TriDye 1kb Plus DNA Ladder (cat #N3270S, NEB) was used for size estimation.

4.2.4 MIDIPREP plasmid extraction

Midipreps of positive colonies were performed to isolate plasmid DNA. The concentrations and purity of the isolated high-copy plasmids are shown in the table below.

Table 6. Concentration and purity of extracted plasmid DNA.
Parameters were calculated on Thermo Fisher Scientific Nanodrop 2000c. 260/280 ratio is within optimal range for each plasmid. 260/230 was not optimal for pRG2_sgRNA 1 plasmid, so additional sedimentation with 75% ethanol had been done.

Sample ID	Nucleic Acid, ng/µL	A260 (Abs)	A280 (Abs)	260/280	260/230
pRG2_sgRNA 1	407.1	8.142	4.516	1.80	1.54
pRG2_sgRNA 2	502.7	10.064	5.448	1.85	2.01
pRG2_sgRNA 3	1058.5	21.174	11.396	1.86	2.17
pRG2_sgRNA 4	615.5	12.310	6.623	1.86	2.11

Additional confirmation of the presence of inserted sgRNA in the vector was done with PCR on the same conditions, as previously described (Figure 12).

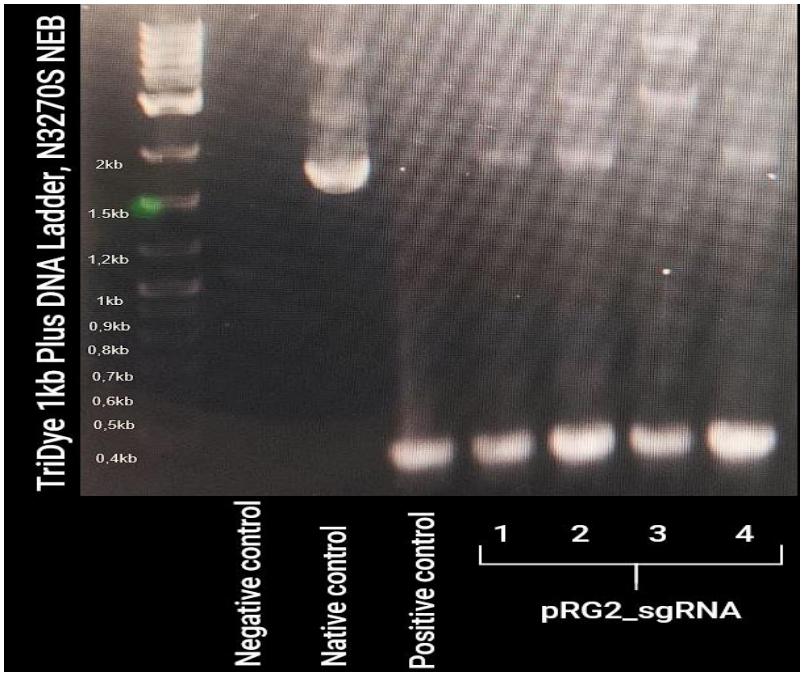

Figure 12. PCR confirmation of sgRNA insertion in extracted pRG2 plasmids after MIDIPREP extraction.
The results of PCR are shown under UV light in 1.5% agarose gel. All samples (sgRNA 1 – 4) produced a single band of the expected size (~400bp), which corresponds to a positive control, indicating the presence of sgRNA construct. TriDye 1kb Plus DNA Ladder (cat #N3270S, NEB) was used for size estimation.

4.2.5 Verification by Restriction Analysis

The extracted pRG2_sgRNA vector was subjected to restriction digestion and analyzed by gel electrophoresis. Both cut and uncut plasmids matched expected sizes compared to the molecular ladder (Figure 13).

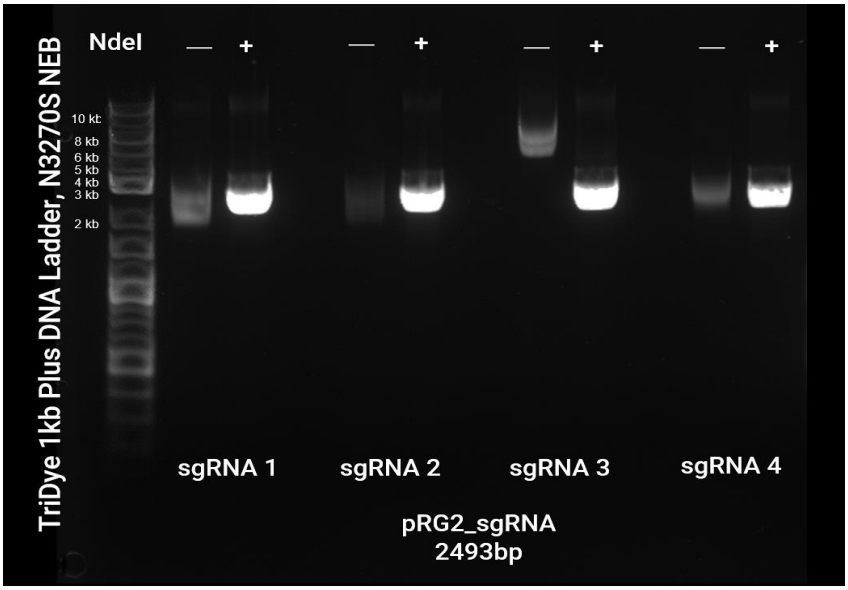

Figure 13. Restriction enzyme digestion analysis of the extracted pRG2_sgRNA constructs.

Agarose gel electrophoresis of plasmid DNA before (–) and after (+) digestion with NdeI. Digestion resulted in the expected band pattern for the pRG2_sgRNA backbone (2493 bp). A TriDye 1 kb Plus DNA Ladder (NEB, N3270S) was used as a molecular weight marker.

4.2.6 Sequencing Confirmation

An additional piece of evidence was provided by sequencing extracted pRG2_sgRNA vectors. Shown below are the aligned sequences of the corresponding sgRNA constructs and ATPA1_G3 plasmid, obtained via the VectorBuilder sequence alignment webtool (https://en.vectorbuilder.com/tool/sequence-alignment.html):

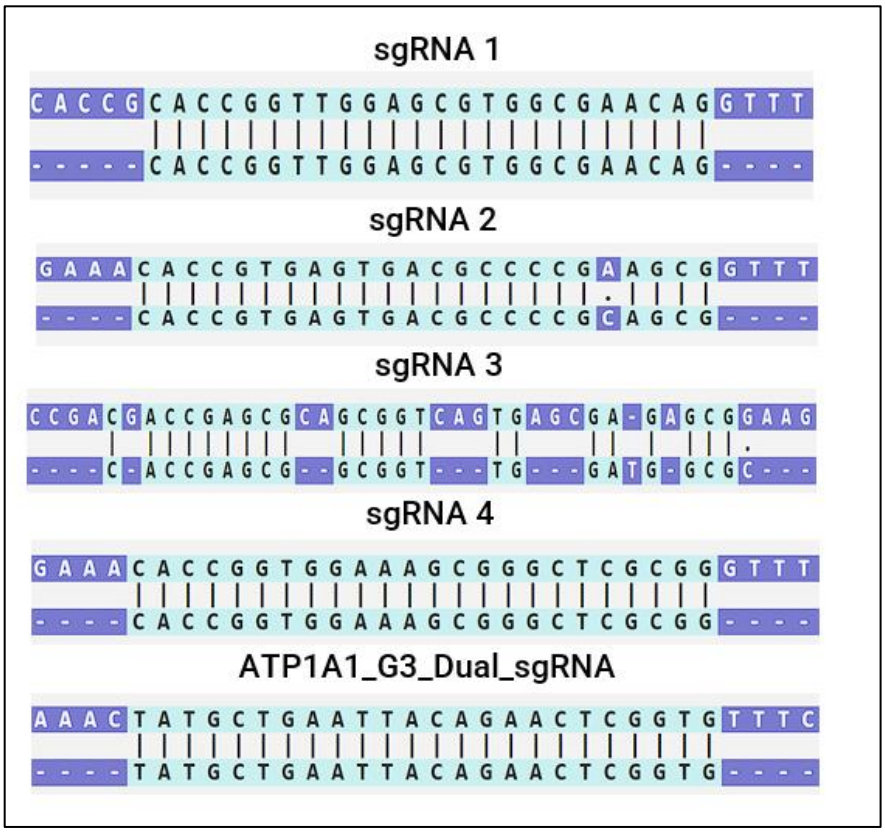

Figure 14.Sequence alignment of obtained plasmid sequences with their respective expected sequences.
Sequencing results (top sequences) for each sgRNA and ATP1A1_G3_Dual_sgRNA plasmids were aligned against their respective expected sequences (bottom sequences). sgRNA 1 and sgRNA 4 showed 100% match with their expected sequences. While sgRNA 2 exhibited a small nucleotide substitution, sgRNA 3 exhibited lots of mismatches, indicating possible sequencing artifacts or mutations present. Due to this, sgRNA 3 was excluded from further screening of H460 cells transfected and selected for ouabain resistance.

4.3 Transfection and Selection of H460 Cells

4.3.1 Morphological Assessment

Microscopy images confirmed the morphology of H460 cells prior to transfection (Figure 15).

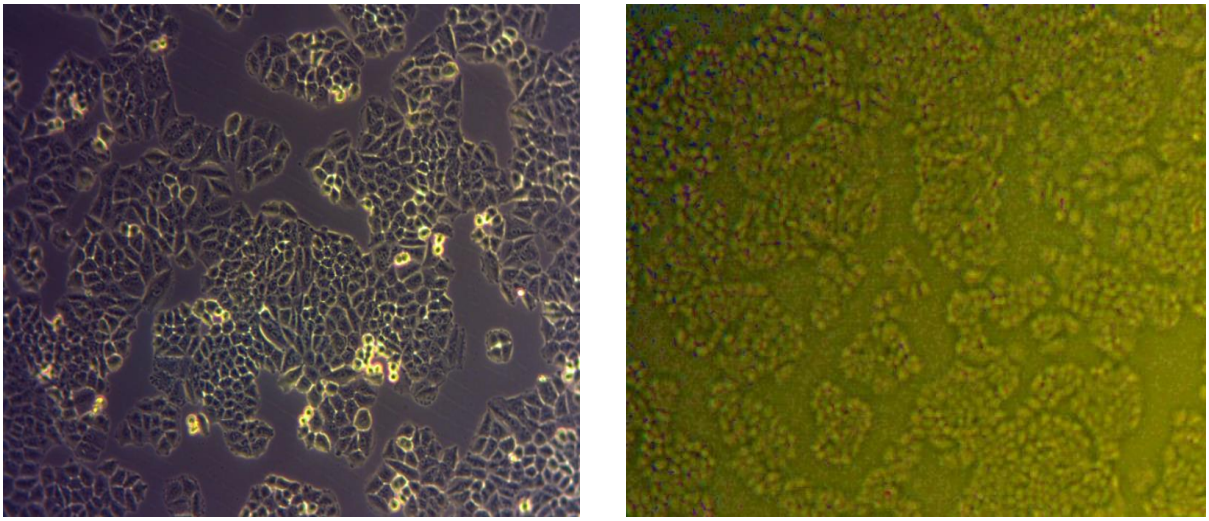

Figure 15. Morphology assessment of H460 cells prior to transfection.
Representative brightfield images of H460 cells before transfection (70-75% confluency). Cells exhibit typical epithelial morphology characterized by a polygonal shape and tight cell-to-cell contacts, indicating healthy and optimal growth conditions for subsequent experimental procedures.

4.3.2 H460 cell line transfection efficiency estimation

Following transfection with the GFP plasmid, fluorescence microscopy revealed successful transfection. GFP-positive cells were visible under fluorescent light (Figure 16), with an estimated transfection efficiency of 30-35%.

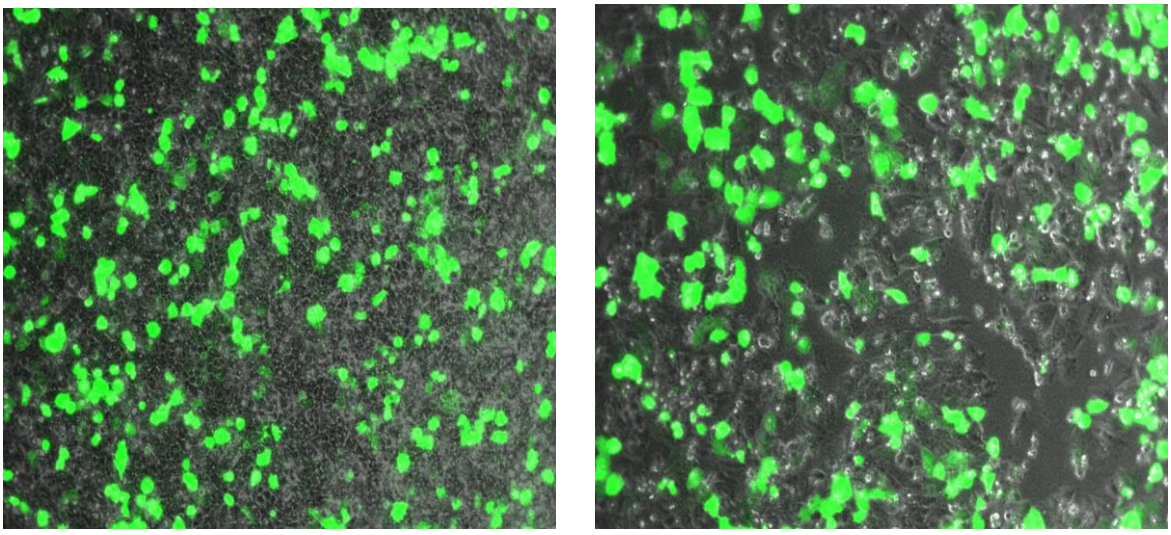

Figure 16. Assessment of transfection efficiency in H460 cells by GFP fluorescence.
Representative merged images of H460 cells expressing GFP after transfection. Successful transfection is indicated by green fluorescence in the cells. Transfection efficiency was estimated based on the proportion of GFP-positive cells relative to the total cell population.

4.3.3 Post Transfection Ouabain Selection

Selection with ouabain was performed to enrich for successfully transfected cells. As expected, cells started dying after treatment, and after 48 hours, there were no live cells observed in the control groups (GFP well, GFP + sgRNA + G3, no Cas9 well).

Surviving colonies were observed on day 4 post-treatment in 0.05µM ouabain concentration in all samples, 0.2µM ouabain concentration only in 2 + 4, 1+4, and 1+2 sgRNA combinations. At the same time, Cas9 + G3 control had colonies in both 0.05 µM and 0.2µM concentrations (Figure 17). Since no positive colonies were observed in 0.5µM ouabain-treated well, it was decided to discard it from further study.

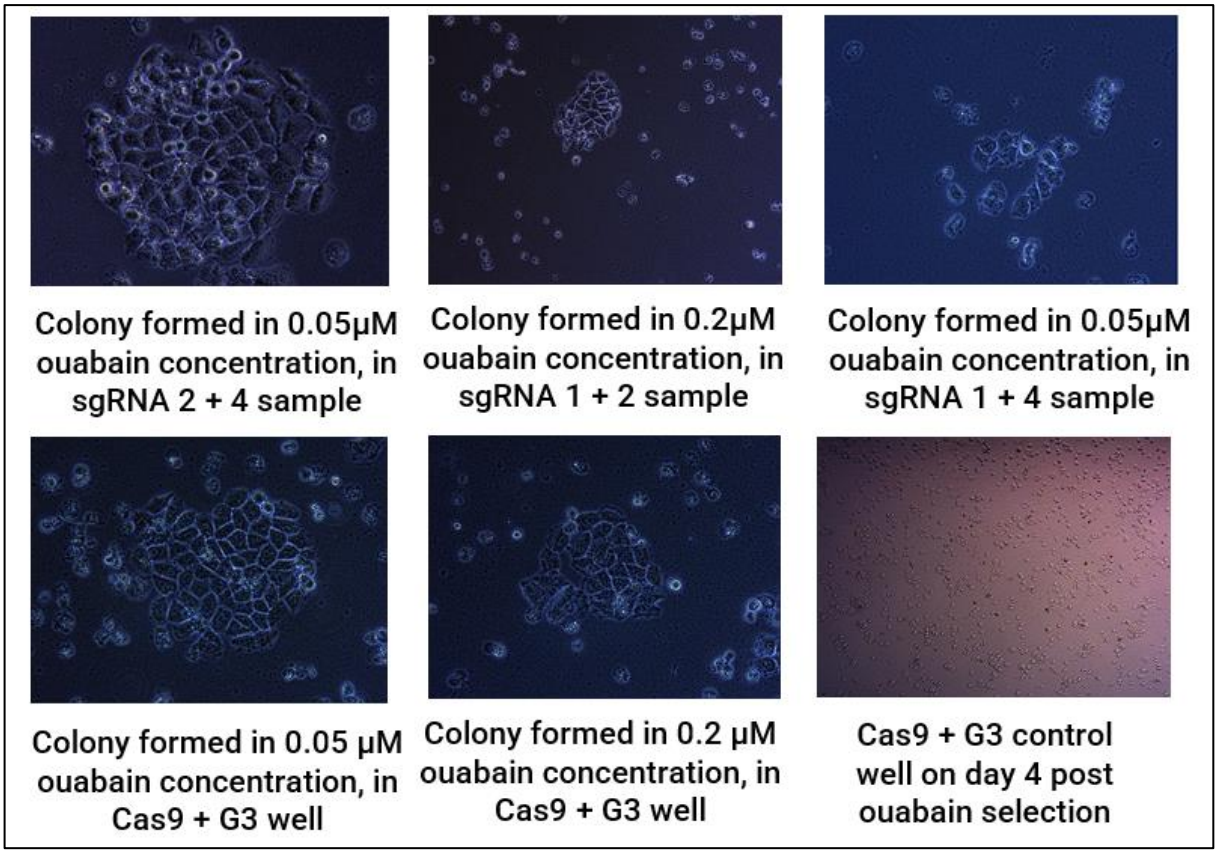

Figure 17. Post transfection ouabain selection.
The positive colonies with ouabain resistance can be seen throughout different samples with different concentrations at day 4 post treatment. From this point, it was decided to let the colonies grow and proliferate for future studies, including PCR analysis. Wells, treated with 0.5µM ouabain octahydrate, did not yield any colonies both in the sample and control (Cas9 + G3) group.

4.3.4 PCR Validation of transfected cells

On day 6 post-transfection, the H460 transfected cells from the untreated group were pooled and subjected to the PCR analysis of CD320 Knockout. As shown in Figure 18, all samples only show a 304bp band, making expression that no deletion has occurred.

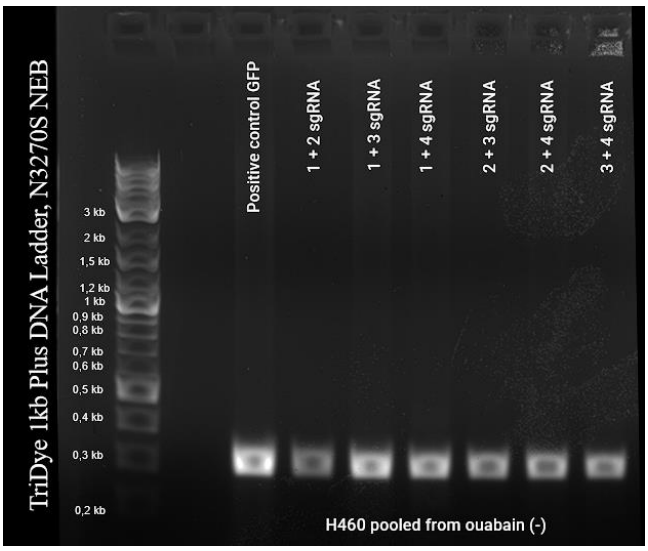

Figure 18. PCR analysis of pooled H460 colonies after CRISPR/Cas9 targeting of the CD320 gene.
PCR products were separated on a 1% agarose gel and visualized under UV light. The expected product size for wild-type (no deletion) is approximately 304 bp. The positive control (PC, GFP plasmid) shows a single band at ~304 bp. No evidence of deletion (i.e., absence of smaller-sized bands) was observed in the sgRNA-transfected samples (samples 1+2, 1+3, 1+4, 2+3, 2+4, and 3+4), indicating unsuccessful or incomplete editing. TriDye 1kb Plus DNA Ladder (N3270S, NEB) was used for size estimation.

However, the results of the PCR validation of ouabain-positive selected colonies are more promising. As shown in Figure 18, colonies № 2 and № 3 from the 2+4 sgRNA combination may carry CD320 KO cells. Two band formations suggest the heterogeneity of the colony. The size of the additional band also complies to the expected deletion size (~240bp).

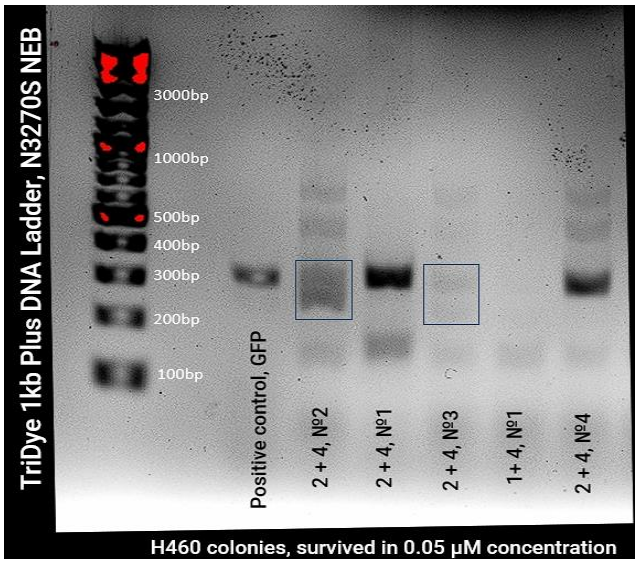

Figure 19. PCR analysis of single H460 colonies, survived in 0.05μM ouabain octahydrate concentration.
PCR products were separated on a 2% agarose gel and visualized under UV light. Expected product size for willd-type CD320 is 304bp. Wells with 2+4 sgRNA combination, colonies № 2 and № 3 show an additional band. Since it complies to the expected deletion size (240bp product), the colony might carry CD320 KO cells. TriDye 1kb Plus DNA Ladder (N3270S, NEB) was used for size estimation.

5. Discussion

In this study, we aimed to establish a CD320 Knockout in the H460 cell line using CRISPR/Cas9 approach and ouabain co-selection. Our results showed that despite the fact that transfection was indeed successful and selection with ouabain effectively eliminated non-resistant cells, no clear evidence of CD320 gene deletion was observed in the untreated group.

The main possible explanation for these could be the essentiality of the CD320 gene for cell survival. To overcome this problem, one might consider the overexpression of the LRP2 receptor protein, which also facilitates the uptake of transcobalamin. Co-transfecting cells with an LRP2-expressing plasmid or establishing stable LRP2 overexpression lines prior to experimental transfection may increase internalization of DNA complexes and improve the survival of edited CD320-deficient cells.

Nevertheless, other study report CD320 conditional knockout in mice (Bernard et al., 2018), and there are commercially available cell lineages by EditGene and Ubigene, which carry knockout of genes like Hep G2, HCT 116, 293T, A549, and other cell lines. However, there are no reports on the non-small cell lung cancer cell lines with this mutation.

Another contributing factor could be the limited efficiency of Lipofectamine 2000-mediated transfection in H460 cells. Low delivery rates of the plasmids could have reduced the probability of generating effective knockouts. Additionally, the number of plasmids delivered into cell could have also affected overall transfection efficiency. In future experiments, a more efficient strategy would be to clone sgRNA directly into an ATPA1_G3_dual_sgRNA plasmid, which will confer resistance to ouabain at the same time. Another possible option is to create all-one plasmid, expressing Cas9, sgRNA against the target gene, and ATPA1, under the one promoter. However, in that case, the size of the plasmid would be too big for cells to handle, and we would definitely need to rely on other means of transfection (like electroporation).

Selection with ouabain is an efficient method for enriching transfected cells. However, it is worth mentioning that our finding differs slightly from those reported by Agudelo et al. (2017), who recommended 0.5µM ouabain octahydrate as an optimal concentration for effective selection. In our hands, no surviving colonies were observed at that concentration, suggesting the higher sensitivity of H460 cells to ouabain, possibly due to intrinsic variability in Na^+/K^+-ATPase expression levels or cellular stress responses. At the same time, there was a deviation from the provided protocol, since we diluted ouabain octahydrate in DMSO, instead of the water, how it was originally suggested.

Based on the current findings, the next step of the study will involve dilution of positive 2+4, №2, and 3 colonies to single cells and expansion in 96-well plates. Since the cell lineage in the study contains wild-type p53, it would be a great control for qPCR analysis and Western blots in the future.

Finally, the sgRNA design, along with ouabain selection strategy and optimized transfection conditions in this study, can be directly applied to other cell lines, including H1975, to further investigate the interplay between CD320 and TP53 GOF mutations. The successful establishment of CD320-deficient in vitro models will provide a crucial tool for unraveling the biological relationship between vitamin B12 uptake pathways and tumor suppressor signaling in NSCLC. On the last note, the analysis of the effect of CD320 KO on cell proliferation rate in cell lines with varying TP53 status, H460 bearing wt p53, and H1975 with mut p53, was not achieved due to the time limitation.

6. Reference list

Agudelo, D., Duringer, A., Bozoyan, L. et al. Marker-free coselection for CRISPR-driven genome editing in human cells. Nat Methods 14, 615–620 (2017). https://doi.org/10.1038/nmeth.4265

Alam, S. K., Yadav, V. K., Bajaj, S., Datta, A., Dutta, S. K., Bhattacharyya, M., Bhattacharya, S., Debnath, S., Roy, S., Boardman, L. A., Smyrk, T. C., Molina, J. R., Chakrabarti, S., Chowdhury, S., Mukhopadhyay, D., & Roychoudhury, S. (2016a). DNA damage-induced ephrin-B2 reverse signaling promotes chemoresistance and drives EMT in colorectal carcinoma harboring mutant p53. *Cell Death & Differentiation*, 23, 707-722. https://doi.org/ 10.1038/cdd.2015.133

Alam, A., Woo, J.-S., Schmitz, J., Prinz, B., Root, K., Chen, F., Bloch, J. S., Zenobi, R., & Locher, K. P. (2016b). Structural basis of transcobalamin recognition by human CD320 receptor. *Nature Communications*, *7*(1). https://doi.org/10.1038/ncomms12100

Alvarado-Ortiz, E., de la Cruz-López, K. G., Becerril-Rico, J., Sarabia-Sánchez, M. A., Ortiz-Sánchez, E., & García-Carrancá, A. (2021). Mutant p53 gain-of-function: Role in cancer development, progression, and therapeutic approaches. *Frontiers in Cell and Developmental Biology*, 8, Article 607670. https://doi.org/10.3389/fcell.2020.607670

Attardi, L.D., Boutelle, A.M. Targeting p53 gain-of-function activity in cancer therapy: a cautionary tale. *Cell Death Differ* **31**, 133–135 (2024). https://doi.org/10.1038/s41418-023-01253-7

Baker, S. J., Markowitz, S., Fearon, E. R., Willson, J. K., & Vogelstein, B. (1990). Suppression of human colorectal carcinoma cell growth by wild-type p53. *Science (New York, N.Y.)*, *249*(4971), 912–915. https://doi.org/10.1126/science.2144057

Bernard, D. J., Pangilinan, F. J., Cheng, J., Molloy, A. M., & Brody, L. C. (2018). Mice lacking the transcobalamin-vitamin B12 receptor, CD320, suffer from anemia and reproductive deficits when fed vitamin B12-deficient diet. Human molecular genetics, 27(20), 3627–3640. https://doi.org/10.1093/hmg/ddy267

Chen, X., Zhang, T., Su, W., Dou, Z., Zhao, D., Jin, X., Lei, H., Wang, J., Xie, X., Cheng, B., Li, Q., Zhang, H., & Di, C. (2022). Mutant p53 in cancer: from molecular mechanism to therapeutic modulation. Cell death & disease, 13(11), 974. https://doi.org/10.1038/s41419-022-05408-1

Dittmer, D., Pati, S., Zambetti, G., Chu, S., Teresky, A. K., Moore, M., Finlay, C., & Levine, A. J. (1993). Gain of function mutations in p53. *Nature genetics*, *4*(1), 42–46. https://doi.org/10.1038/ng0593-42

Dolma, L., & Muller, P. A. J. (2022). *GOF mutant p53 in cancers: A therapeutic challenge*. *Cancers*, *14*(20), 5091. https://doi.org/10.3390/cancers14205091

Elzi, D. J., Bauta, W., Lai, S.-C., Das, T., Mogare, S., & Rebel, V. I. (2021). Simultaneous knockdown of CD320 and LRP2 receptors is selectively toxic to cancer cells but not normal cells. *Cancer Research*, 81(13_Supplement), 1223. https://doi.org/10.1158/1538-7445.AM2021-1223

Eliyahu, D., Michalovitz, D. & Oren, M. Overproduction of p53 antigen makes established cells highly tumorigenic. *Nature* **316**, 158–160 (1985). https://doi.org/10.1038/316158a0

Gick, G. G., Arora, K., Sequeira, J. M., Nakayama, Y., Lai, S. C., & Quadros, E. V. (2020). Cellular uptake of vitamin B_{12}: Role and fate of TCblR/CD320, the transcobalamin receptor. *Experimental cell research*, *396*(1), 112256. https://doi.org/10.1016/j.yexcr.2020.112256

Joerger, A. C., & Fersht, A. R. (2007). Structural biology of the tumor suppressor p53 and cancer-associated mutants. *Advances in cancer research*, *97*, 1–23. https://doi.org/10.1016/S0065-230X(06)97001-8

Joyce, C., Rayi, A., & Kasi, A. (2023, August 28). Tumor-suppressor genes. In *StatPearls* (Internet). StatPearls Publishing. https://www.ncbi.nlm.nih.gov/books/NBK532243/

Kastenhuber, E. R., & Lowe, S. W. (2017). Putting p53 in context. *Cell*, *170*(6), 1062–1078. https://doi.org/10.1016/j.cell.2017.08.028

Lai, S.-C., Nakayama, Y., Sequeira, J. M., & Quadros, E. V. (2011). Down-regulation of transcobalamin receptor TCBLR/CD320 by siRNA inhibits cobalamin uptake and proliferation of cells in culture. *Experimental Cell Research*, 317(11), 1603-1607. https://doi.org/10.1016/j.yexcr.2011.02.016

Lang, G. A., Iwakuma, T., Suh, Y. A., Liu, G., Rao, V. A., Parant, J. M., ... & Lozano, G. (2004). Gain of function of a p53 hot spot mutation in a mouse model of Li-Fraumeni syndrome. *Cell*, *119*(6), 861–872. https://doi.org/10.1016/j.cell.2004.11.006

Liu, D. P., Song, H., & Xu, Y. (2010). A common gain of function of p53 cancer mutants in inducing genetic instability. *Oncogene*, *29*(7), 949–956. https://doi.org/10.1038/onc.2009.376

Mogi, A., & Kuwano, H. (2011). TP53 mutations in nonsmall cell lung cancer. *BioMed Research International*, 2011, Article 583929. https://doi.org/10.1155/2011/583929

Olive, K. P., Tuveson, D. A., Ruhe, Z. C., Yin, B., Willis, N. A., Bronson, R. T., Crowley, D., & Jacks, T. (2004). Mutant p53 gain of function in two mouse models of Li-Fraumeni syndrome. *Cell*, *119*(6), 847–860. https://doi.org/10.1016/j.cell.2004.11.004

Olivier, M., Hollstein, M., & Hainaut, P. (2010). TP53 mutations in human cancers: Origins, consequences, and clinical use. *Cold Spring Harbor Perspectives in Biology*, 2(1), Article a001008. https://doi.org/10.1101/cshperspect.a001008

Oren, M., & Prives, C. (2024). p53: A tale of complexity and context. *Cell*, *187*(7), 1569–1573. https://doi.org/10.1016/j.cell.2024.02.043

Quadros, E. V., & Sequeira, J. M. (2013). Cellular uptake of cobalamin: transcobalamin and the TCblR/CD320 receptor. *Biochimie*, *95*(5), 1008–1018. https://doi.org/10.1016/j.biochi.2013.02.004

Sabapathy, K., & Lane, D. P. (2018). Therapeutic targeting of p53: all mutants are equal, but some mutants are more equal than others. *Nature reviews. Clinical oncology*, *15*(1), 13–30. https://doi.org/10.1038/nrclinonc.2017.151

Sasaki, K., Takahashi, S., Ouchi, K., Otsuki, Y., Wakayama, S., & Ishioka, C. (2023). Different impacts of TP53 mutations on cell cycle-related gene expression among cancer types. *Scientific reports*, *13*(1), 4868. https://doi.org/10.1038/s41598-023-32092-8

Shah, S., Roth, A., Goya, R. et al. The clonal and mutational evolution spectrum of primary triple-negative breast cancers. *Nature* 486, 395–399 (2012). https://doi.org/10.1038/nature10933

Shaulsky, G., Goldfinger, N., Peled, A., & Rotter, V. (1991). Involvement of wild-type p53 in pre-B-cell differentiation in vitro. *Proceedings of the National Academy of Sciences of the United States of America*, *88*(20), 8982–8986. https://doi.org/10.1073/pnas.88.20.8982

Stein, Y., Rotter, V., & Aloni-Grinstein, R. (2019). Gain-of-Function Mutant p53: All the Roads Lead to Tumorigenesis. *International journal of molecular sciences*, *20*(24), 6197. https://doi.org/10.3390/ijms20246197

Tong D. R., Zhou W., Katz C., Regunath K., Venkatesh D., Ihuegbu C., et al. (2021). p53 Frameshift Mutations Couple Loss-Of-Function with Unique Neomorphic Activities. *Mol. Cancer Res*. *19*, 1522–1533. https://doi.org/10.1158/1541-7786.mcr-20-0691

Valenti, F., Ganci, F., Fontemaggi, G., Sacconi, A., Strano, S., Blandino, G., & Di Agostino, S. (2015). Gain of function mutant p53 proteins cooperate with E2F4 to transcriptionally downregulate RAD17 and BRCA1 gene expression. *Oncotarget*, *6*(8), 5547–5566. https://doi.org/10.18632/oncotarget.2587

Wang, H., Guo, M., Wei, H. et al. Targeting p53 pathways: mechanisms, structures and advances in therapy. *Sig Transduct Target Ther* 8, 92 (2023). https://doi.org/10.1038/s41392-023-01347-1

Wolf, D., Harris, N., Goldfinger, N., & Rotter, V. (1985). Isolation of a full-length mouse cDNA clone coding for an immunologically distinct p53 molecule. *Molecular and cellular biology*, *5*(1), 127–132. https://doi.org/10.1128/mcb.5.1.127-132.1985

Zhang, C., Liu, J., Xu, D., Zhang, T., Hu, W., & Feng, Z. (2020). Gain-of-function mutant p53 in cancer progression and therapy. *Journal of molecular cell biology*, *12*(9), 674–687. https://doi.org/10.1093/jmcb/mjaa040

Zhang, C., Liu, J., Liang, Y., Wu, R., Zhao, Y., Hong, X., Lin, M., Yu, H., Liu, L., Levine, A. J., Hu, W., & Feng, Z. (2013). Tumour-associated mutant p53 drives the Warburg effect. *Nature communications*, *4*, 2935. https://doi.org/10.1038/ncomms3935